GEOLOGICA CARPATHICA, 2026, 77, 1, 17–42 https://doi.org/10.31577/GeolCarp.2026.01

Petrology and geochemistry of hydrothermal alteration types at the Elatsite porphyry-copper deposit (Bulgaria)

HRISTIANA GEORGIEVA[1,✉], ROSSEN NEDIALKOV[2], ELITSA STEFANOVA[1], GEORGI MILENKOV[1], ZAHARI NANOV[2], IVAN KRUMOV[2], NEVEN GEORGIEV[2] and PETROSLAV PETROV[3]

[1]Geological Institute, Bulgarian Academy of Sciences, Department of Geochemistry and Petrography, Acad. G. Bonchev str., 1113 Sofia, Bulgaria
[2]Sofia University "St. Kliment Ohridski", Departament of Mineralogy, Petrology and Economic Geology, 15 Tsar Osvoboditel Blvd., 1504 Sofia, Bulgaria
[3]Elatsite-MED AD, Etropole 2180, Sofia district, Bulgaria

(Manuscript received July 9, 2025; accepted in revised form February 4, 2026; Associate Editor: Peter Koděra)

Abstract: The formation of the Elatsite deposit is related to the emplacement of several Upper Cretaceous porphyritic intrusions with the most significant intrusions of quartz-monzodiorite and granodiorite porphyries. The surface exposure of the Elatsite deposit provides an opportunity for investigating the lithogeochemical features of different hydrothermal alteration types. Petrographic observation combined with detailed geochemical analysis of the hydrothermal alteration types and chemical features of secondary biotite, amphibole, plagioclase and chlorite, led to the assessment of gains and losses of major, trace and REE elements and the origin of fluids for the variety of alterations. The Na–Ca alteration is probably formed from a mixture of magmatic and external fluids. The Na–Ca–K-silicate alteration is formed during fluid–fluid interaction of magmatic and external fluid, with predominance of the magmatic one, and occurs in the zone of primary neutralization. The K-silicate alteration is formed by magmatic fluids with a high oxygen fugacity, high temperature, high a_{K+} and a_{Mg2+}. The upward superimposition of the K-silicate–sericitic alteration is related to the incorporation of meteoric fluids into magmatic fluids in an initial high oxygen fugacity environment and a high a_{Mg2+}. The quartz–sericitic alteration occurs from admixture of meteoric fluid into evolving magmatic fluids, with the predominance of the meteoric fluid, inducing an environment with a low a_{K+}/a_{H+} ratio. The quartz–adularia–carbonate alteration is probably resulting of the admixture of a magmatic fluid with external and meteoric fluids, in an environment with high a_{K+}. The propylitic alteration is observed only in the periphery zones of the deposit and clear relations with other alteration types were not observed.

Keywords: porphyry-copper deposits, hydrothermal alterations, geochemistry, Elatsite

Introduction

Porphyry-copper deposits are one of the biggest sources of Cu, Au and Mo. The open-pit mining method allows for relatively inexpensive ore extraction, making these types of deposits among the most extensively studied in the world. Scientific approaches consider the ore deposition as a part of the overall hydrothermal process within the magmatic-hydrothermal system operating in the porphyry-copper deposits. This makes the understanding of the fluid-rock interaction conditions important for the comprehensive study of the ore deposition (e.g., Panigrahi et al. 2008; Kanazirski 2011; Afshooni et al. 2013).

Hydrothermally altered rocks are volumetrically the most significant product of the magmatic-hydrothermal system (e.g., Kanazirski 2011). Their formation includes compositional changes of major and trace element geochemistry, mineralogy, stable isotope composition. (e.g., Dilles & Einaudi 1992; Dilles et al. 1992, 1995; Idrus et al. 2009; Davies & Whitehead 2010). All these variables are covered in models for the spatial and temporal distribution of hydrothermal alteration products associated with porphyry-copper deposits, suggested by numerous authors (e.g., Lowell & Guilbert 1970; Hollister 1978; Seedorff et al. 2005, 2008; Sinclair 2007; Sillitoe 2010). Despite the differences between the variety of models, in general the deep and central parts of the system are defined by fluid-rock interaction of early, magmatic, hot fluid. This leads to the formation of a potassic alteration core with transition to a propylitic alteration halo around it. Upwards the mixing of meteoric and magmatic fluids that interact with the host-rock results in superimposition of chlorite–sericitic, sericitic and argillic alteration (e.g., Lowell & Guilbert 1970; Sinclair 2007; Seedorff et al. 2008; Sillitoe 2010). According to the different models, two to three sources of components are responsible for the formation of hydrothermal fluids, and most significant are magmatic and meteoric fluids. There are some different opinions on the source of components for sodium–calcic alteration (e.g., Seedorff et al. 2008), as some determine its synchronous formation with potassium silicate alteration, by saline, non-magmatic, hot fluids (e.g., Norton 1978; Dilles

✉ corresponding author: Hristiana Georgieva
ch_georgieva@geology.bas.bg

& Einaudi 1992; Dilles et al. 1995), while others consider magmatic origin (e.g., Lang et al. 1995). As commented in Dilles & Einaudi (1992), although much information is already collected about the porphyry-copper deposits, a gap exists in limited exposures of both the tops and bottoms of the same hydrothermal system and it is possible that the view for two main hydrothermal fluid sources (magmatic and meteoric) is simplistic. The multiple sources of hydrothermal fluids in the porphyry-copper systems are still a debating question. In this sense the Elatsite mine is an excellent object for investigation of the hydrothermal alteration zonation and its features and sources. The surface exposure of the deposit provides an opportunity to study the bottom, central and middle parts of the system enabling the description of nearly all hydrothermal alteration types typical for porphyry copper deposit models.

The compositional changes of major element geochemistry of some hydrothermal alteration types, some mineralogical changes and fluid inclusions study of quartz samples from different ore minerals associations at the Elatsite deposit have been object of investigation (e.g., Strashimirov et al. 2002; Tarkian et al. 2003; Kehayov 2005; Georgiev 2008, 2019; Stefanova et al. 2014; Fekete et al. 2016; Georgieva et al. 2019). According to data for the genesis and evolution of the deposit, the begging of the hydrothermal activity at the deposit starts after the intrusion of quartz-monzodiorite porphyry, with formation of magmatic-hydrothermal breccias and quartz–magnetite veining accompanied by the K-silicate alteration and intensive alteration of the wall rocks (e.g., Strashimirov et al. 2002; Hadzhieva 2009; Stefanova et al. 2014). The K-silicate alteration is characterized as pre-ore main mineralization stage of hydrothermal activity formed by early magmatic fluids with a limited admixture of meteoric fluids and formation of secondary biotite, potassium feldspar, quartz, illite, plagioclase, and calcite replacing primary minerals (biotite, amphibole, potassium feldspar), and relatively high values for a_{K+}/a_{H+} of the solutions (Strashimirov et al. 2002; Georgiev 2008, 2019; Stefanova et al. 2014). Intermediate-density fluid inclusions in quartz from earliest quartz veins associating with K-silicate alteration are described with 5.9–8.9 wt% NaCl eq., 2 mol% CO_2, temperature of homogenization about 640 °C, at 1 kbar and estimated depth of formation 4–5 km (Stefanova et al. 2014). The K-silicate–sericitic alteration is defined with the presence of chlorite, sericite, quartz, pyrite, and chalcopyrite assemblage (Strashimirov et al. 2002; Georgiev 2019). The quartz–sericitic alteration occurs in pre- to post-ore main mineralization stages with development of quartz–illite–pyrite assemblage from fluids with low salinity (Strashimirov et al. 2002; Georgiev 2008). Propylitic alteration is related to a later hydrothermal impulse with chloritization, epidotization, sericitization, actinolitization (Bogdanov 1987; Strashimirov et al. 2002; Georgiev 2019). Aqueous liquid inclusions in quartz associated with zeolite, carbonate, chlorite mineral assemblage indicate 143–147 °C temperature of homogenization and 3.7±0.5 wt% NaCl eq. of the corresponding fluids (Stefanova et al. 2014).

Our paper discusses the whole-rock (major and trace element) geochemistry of the alteration types at the Elatsite deposit and some chemical features of secondary minerals, combining the previously published data for the evolution of the deposit with new detailed petrological and geochemical features of the rocks, linking the fluid composition with the hydrothermal alteration types in a united model for the zonation of hydrothermal alteration types and the evolution of magmatic-hydrothermal system at the deposit.

Geological setting

Basement and Late Cretaceous porphyries

The Elatsite porphyry copper deposit (PCD) is located at the northernmost area of the Panagyurishte ore region in the segment of Srednogorie zone, part of the Apuseni–Banat–Timok–Srednogorie magmatic and metallogenic belt (e.g., Ciobanu et al. 2002; Popov et al. 2002, Fig.1). The deposit is hosted in the apical parts of subvolcanic to hypabyssal Upper Cretaceous intrusions, basement composed of Carboniferous Vezhen pluton and metasediments of Paleozoic age (e.g., Kalaidzhiev et al. 1984; Janković et al. 1997; Ciobanu et al. 2002; Kamenov et al. 2002; Strashimirov et al. 2002; von Quadt et al. 2002; Georgiev S. et al. 2020, Fig. 2). The main factor controlling the emplacement of the Upper Cretaceous subvolcanic bodies is the Kashana reverse fault (e.g., Antonov & Jelev 2002; Georgiev 2004; Popov et al. 2012), one of the main tectonic structures associated with the Alpine evolution of the area (e.g., Gerdjikov & Georgiev 2006; Lazarova et al. 2006; Gerdjikov et al. 2023).

The metamorphic basement rocks of the Elatsite area are represented by phyllites to green schists, referred to the Diabase–Phyllitoid Formation by Trashliev (1961). They are observed in southern parts of the deposit, dominanted by sericitic, chlorite–sericitic schists and phyllites, alternating randomly with layers of metaaleurolites to calcschists. The metamorphic rocks have undergone a contact metamorphism during the emplacement of the Vezhen pluton and a variety of hornfelses, hornfels schists, knotted schists, contact amphibolites, two-mica schists have been formed (e.g., Trashliev 1961; Lazarova 2008).

The rocks of the Vezhen pluton are exposed in the central and northern parts of the deposit. They are represented by amphibole–biotite to biotite–amphibole granodiorites, monzogranites to granites, with a predominance of granodiorites (e.g., Kalaidzheiv et al. 1984; Kamenov et al. 2002; Lazarova 2008). Rare occurrence of quartz-monzodiorites, quartz-diorites, diorites and variety of porphyritic rocks (microgabbro porphyries, gabbro-diorites porphyries, diorite porphyries, granodiorite porphyries, granite porphyries), and aplites have also been identified (e.g., Kalaidzheiv et al. 1984; Kamenov et al. 2002; Lazarova et al. 2006; Lazarova 2008; Popov et al. 2012; Popov & Popov 2022). This suite of rocks has been classified as a high-K Ca-alkaline series by Kamenov et al. (2002).

In the pluton a variety of microgranular magmatic inclusions are described as amphibole gabbro, amphibole diorites and monzodiorites indicating magma mixing (Kamenov et al. 2002; Lazarova 2008). The age of the Vezhen pluton is estimated at about 307±0.85–314±4.8 Ma using U–Pb age dating of zircons (Kamenov et al. 2002; Georgiev S. et al. 2020).

The mineralization and hydrothermal activity in the deposit are related to the emplacement of Late Cretaceous magmatic rocks, represented by a variety of subvolcanic to hypabyssal bodies (e.g., Strashimirov et al. 2002). The magmatic activity starts with the emplacement of quartz-monzodiorite porphyries, followed by the emplacement of variety of porphyritic dykes: granodiorite, diorite, monzodiorite, quartz-syenite, microdiorite, micromonzodiorite, quartz-diorite, and aplites (e.g., Kalaidzhiev et al. 1984; von Quadt et al. 2002, 2005). Different age determinations for the porphyritic rocks have been proposed (e.g., Lilov & Chipchakova 1999; von Quadt et al. 2002; Zimmerman et al. 2003; Handler et al. 2004; Lips et

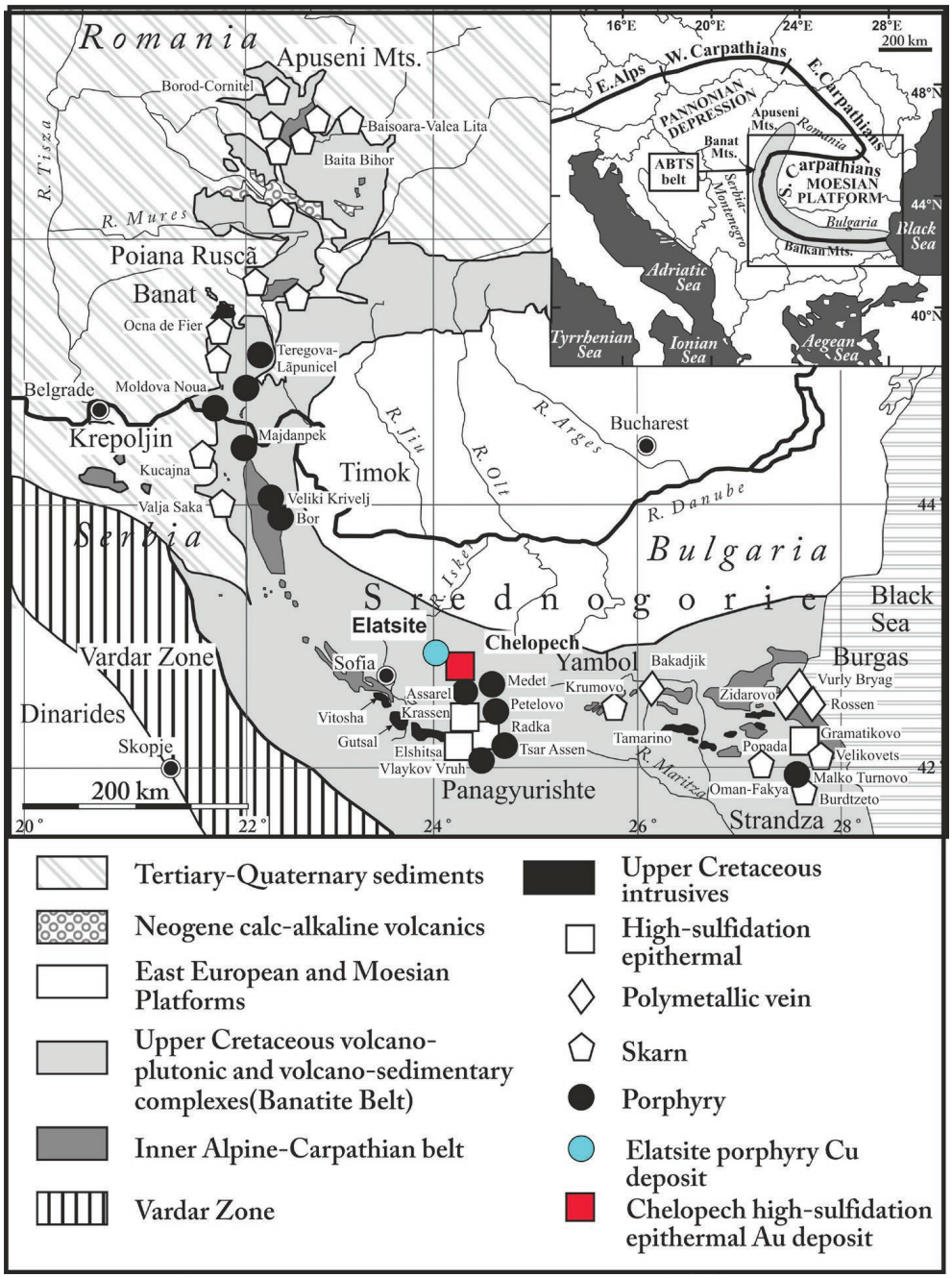

Fig. 1. Geological sketch map of Late Cretaceous magmatic provinces and distribution of main types of ore deposits in the Apuseni–Banat–Timok–Srednogorie (ABTS) belt (modified from Ciobanu et al. 2002, in Stefanova et al. 2023). Inset: Location of the ABTS belt within the Alpine–Balkan–Carpathian–Dinaride orogenic system (after Heinrich & Neubauer 2002, in Stefanova et al. 2023).

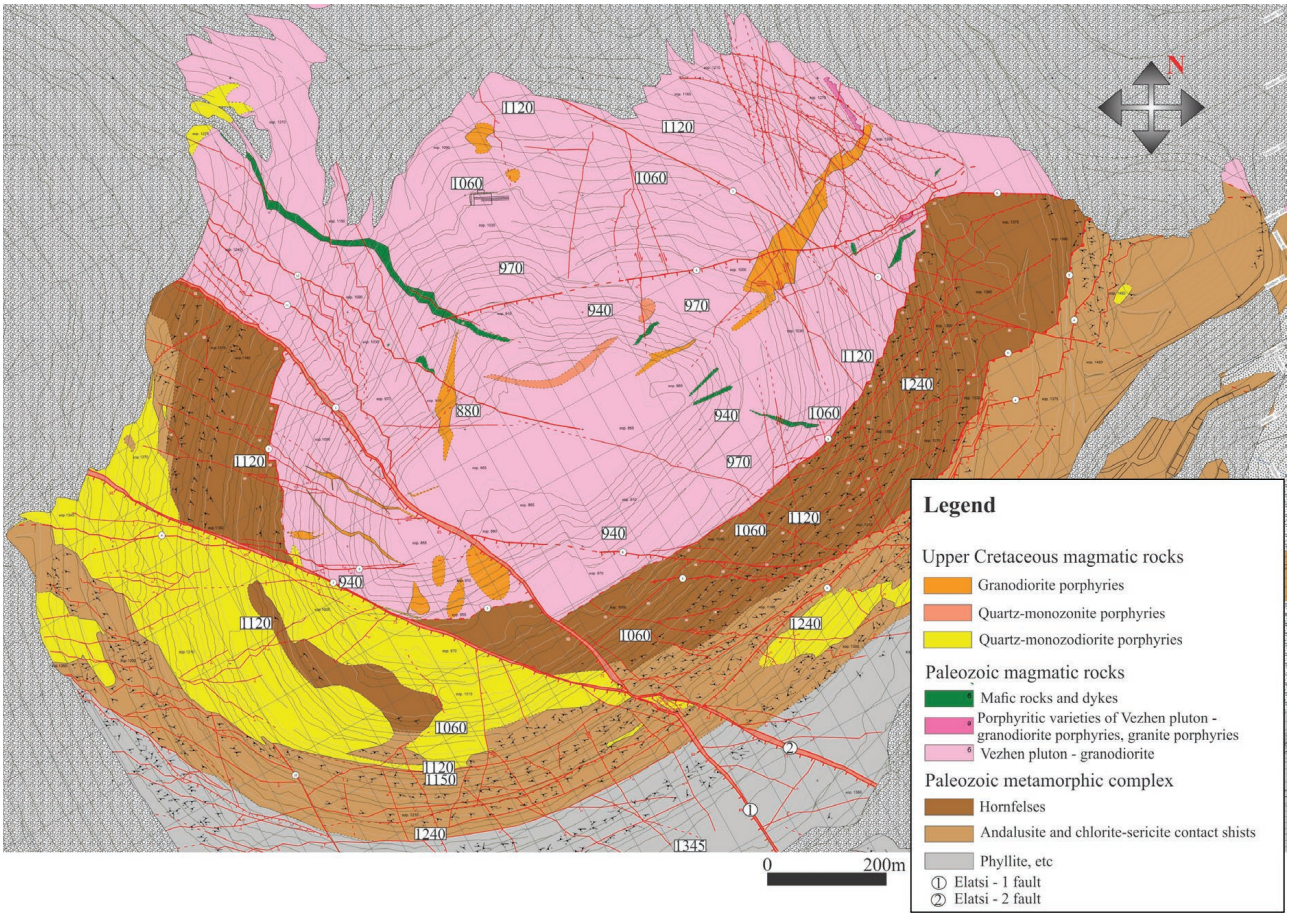

Fig. 2. Geological map of the Elatsite porphyry copper deposit within the open pit mining area (after Georgiev et al. 2023). Rectangles: horizon numbers.

al. 2004), the last one showed the age 92.329±0.021 Ma for monzodiorite porphyries, 92.079±0.026 Ma for granodiorite porphyries, and 92.050±0.019 Ma for aplites (Peytcheva et al. 2015, 2017a, b). Geochemical discrimination suggests that all Cretaceous porphyritic rocks from the Elatsite area are result from enriched mantle source with crustal contamination (von Quadt et al. 2002).

Hydrothermal alteration types and mineralization

Nine different hydrothermal alteration types are described at the Elatsite deposit – Na–Ca, Na–Ca–K-silicate, K-silicate, K-silicate–sericitic (potassium–sericitic), sericitic (quartz–sericitic), propylitic, phyllic–argillic/argillic/argillic-like, quartz–adularia–carbonate and Ca-alteration (e.g., Popov et al. 2000; Kanazirski et al. 2002; Strashimirov et al. 2002, 2003; Kehayov 2005; Georgiev 2008, 2019; Nedialkov et al. 2012; Ivanov et al. 2014; Roman Alday et al. 2018; Georgieva et al. 2019; Roman Alday 2019), which have very complex and ambiguous relationships among them.

The *Na–Ca alteration* is represented by veins with variable mineral content or uniformly distributed secondary amphibole (Georgieva et al. 2019). The distribution of the *Na–Ca–K-silicate alteration* is observed only in granodiorite porphyries in the central and eastern parts of the deposit. The alteration includes secondary biotite and amphibole. The assemblage of quartz, potassium feldspar, biotite, actinolite, carbonate, apatite, titanite, clays minerals, sericite and adularia are described as a mixed Ca–K alteration (Georgiev 2019). The *K-silicate alteration* is distributed in all lithological varieties, but widespread and with higher intensity it is in the rocks of the Vezhen pluton (Fig. 3). Age of the alteration using the Rb–Sr method on secondary biotite is 90.55+0.8 Ma (von Quadt et al. 2002). The formation of the K-silicate alteration is the product of dominantly magmatic fluids at an early stage of hydrothermal evolution (e.g., Strashimirov et al. 2003; Stefanova et al. 2014), with two pulses of formation described at the deposit (Ivanov et al. 2014). The *K-silicate–sericitic alteration* is one of the most abundant types, its spatial distribution is related to the formation of chlorite and sericite accompanying secondary biotite, overprinting the previously formed the K-silicate or Na–Ca–K-silicate alterations (e.g., Kanazirski et al. 2002; Strashimirov et al. 2002; Georgieva & Nedialkov 2021). It is observed with greater intensity in the granodiorites of the Vezhen pluton and in some quartz-monzodiorite porphyries. The *quartz–sericitic alteration* (sericitic)

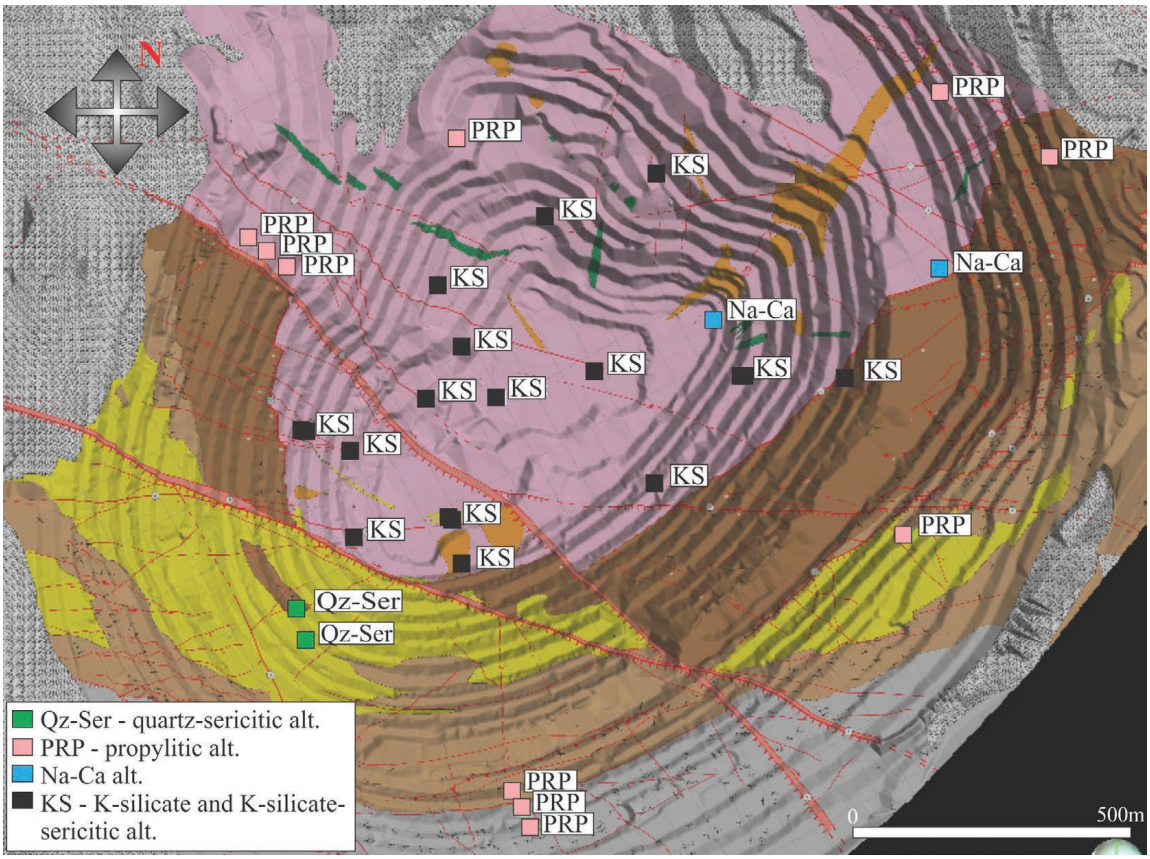

Fig. 3. Generalized map of hydrothermal alterations at the Elatsite deposit (modified after Georgiev N. et al. 2020). Colors of lithologies are the same as in Fig. 2, rectangles show approximately location of samples where the given alteration is described.

alteration is more intense in Late Cretaceous porphyritic rocks from the southern part of the deposit, forming a halo around fractures with mineral assemblage of quartz–illite–pyrite (e.g., Strashimirov et al. 2002; Georgiev 2019). *The propylitic alteration* is a week alteration type occurring mainly in porphyritic rocks. It is observed in peripheral parts of the deposit with mineral association including epidote, chlorite, carbonate minerals and quartz (Strashimirov et al. 2002; Georgiev 2019). The *argillic alteration* is rarely preserved at the deposit, only in SW parts of the open pit, with the mineral assemblage of illite, smectite, chlorite that usually overprints the quartz–sericitic alteration (Kehayov 2005). The *quartz–adularia–carbonate alteration* was described for first time by Nedialkov et al. (2012) in the matrix of magmatic and magmatic-hydrothermal breccias, with the mineral assemblage of adularia, quartz, carbonate, zeolite, and apatite, where the alteration overprints the K-silicate alteration. The *Ca-alteration* is described by the presence of skarns and epidote-rich altered rocks. Skarns are formed in the contact-metamorphosed halo around the Vezhen pluton (Popov et al. 2002; Lazarova 2008), with the mineral assemblage of garnet, epidote, pyroxene, carbonate, prehnite, quartz, amphibole, and sulfides (Georgieva et al. 2023). Epidote-rich altered rocks are rarely preserved at the deposit at the contact of hornfelses and Vezhen pluton, only in the eastern side of the open pit and in some drill holes. They represent an exotic variety of alteration, with mineral assemblages of epidote, prehnite, amphibole, pyroxene, carbonate, plagioclase, and sulfides. The genetic relationship of the Ca-alteration with the Cretaceous hydrothermal activity is not clarified and it is not included in the present study.

At the Elatsite deposit several mineral assemblages are distinguished: quartz–magnetite–bornite/magnetite–bornite–chalcopyrite, quartz–pyrite–chalcopyrite/pyrite–chalcopyrite, quartz–molybdenite, quartz–pyrite, quartz–galena–sphalerite, quartz–calcite–zeolite/carbonate–zeolite (e.g., Petrunov et al. 1992; Dragov & Petrunov 1996; Strashimirov et al. 2002; Tarkian et al. 2003; Augé et al. 2005; Bogdanov et al. 2005; Kehayov 2005; Georgiev 2008, 2019). Quartz–magnetite–bornite/magnetite–bornite–chalcopyrite assemblages correspond to the early stages of mineralization in association with the K-silicate or potassic–propylitic alteration (Petrunov et al. 1992; Dragov & Petrunov 1996; Strashimirov et al. 2002, 2003; Tarkian et al. 2003; Augé et al. 2005; Georgiev 2008; Stefanova et al. 2014; González-Jiménez et al. 2021). Temperatures of formation of the magnetite–bornite–chalcopyrite assemblage are higher than 550 °C (Popov et al. 2000; Kehayov et al. 2003), but some consider temperatures ≤460 °C (Stefanova et al. 2014). Local manifestation of epidote–chlorite–quartz–carbonate alteration (propylitic alteration) is coeval with the magnetite–bornite–chalcopyrite assemblage (Dragov & Petrunov

1996). The economically most important is the quartz–pyrite–chalcopyrite/pyrite–chalcopyrite association, which is associated with the K-silicate–sericitic alteration (Dragov & Petrunov 1996; Strashimirov et al. 2002, 2003), quartz–sericitic alteration or phyllic–argillic alteration (Tarkian et al. 2003; Augé et al. 2005), or propylitic alteration (Georgiev 2008). Quartz–pyrite veins and carbonate–quartz assemblages are affiliated to the post-ore mineralization stage in rocks affected by quartz–sericitic alteration (Dragov & Petrunov 1996; Stefanova et al. 2014).

Materials and methods

The analyses presented in this work are newly obtained data of major and trace element geochemistry of various hydrothermal alteration types and some mineral chemistry features.

Between 2015 to 2024 detailed fieldwork and sampling was done on several horizons (1060, 1090, 1120, 1240, 1345, 1405, 1420) and drill holes from the south, south-east and north sides of the open pit were sampled (GP-48 and GP-56). More than 500 polished thin sections from the open pit and drill holes were examined from altered and unaltered rocks, with well-developed textural characteristics. Standard transmitted and reflected light microscopy was combined for mineral identification and textural correlations between different alteration minerals. The major element content of thirty samples of altered rocks was examined with X-ray fluorescence (XRF) at the Department of Mineralogy, Petrology and Economic geology at the Sofia University, with EDXRF Epsilon 3XLE equipment (PANalytical), and the Omnian 3SW software. The quantitative analysis was conducted by melting of 1 g sample, 3 g $LiBO_2$ and 6 g $Li_2B_4O_7$ as melters. The melt was made in ovens Claisse LeNeo at the temperature of 1063 °C. Loss of ignition is estimated at 1000 °C and it is estimated as a weight percentage of the original sample. The LA-ICP-MS technique was applied to determine minor and trace elements in altered rocks at the laboratory in the Geological Institute of the Bulgarian Academy of Sciences. The LA-ICP-MS (New Wave Research) used was a Perkin Elmer-ELAN DRC-e quadrupole inductively coupled plasma mass spectrometer (Perkin Elmer, Canada) with a New Wave UP193FX LA excimer laser (ATLEX-LR, Germany). The internal standard (SiO_2) was obtained from the XRF of the respective samples, and NIST 610 and NIST 612 were used as external standards. The laser system operated at constant 8 Hz pulse rate and laser energy 1.80–2.60 J/cm^2 on the sample surface of 100 μm spot size. Three analytical measurements were performed in each sample, and their average values were used. Powder X-ray diffraction was used to determine mineral phases in altered rocks (argillic-like alteration and quartz–adularia–carbonate alteration). The XRD patterns were obtained on a Bruker D8 Advance diffractometer, with filtered Co-Kα radiation in range 2θ 4–80°, step 0.02° 2θ, and exposure time per step 1.5 s in the Laboratory of X-ray Diffraction at Department of Mineralogy, Petrology and Economic Geology at the Sofia University.

Normalizations of geochemical analyses were made using the published data of unaltered granodiorites by Kamenov et al. (2002) and of unaltered porphyries by von Quadt et al. (2002). The published data was made using wet chemical analyses in the same laboratory at Sofia University as our results for major elements. A control sample was used for comparison the results and minor differences were determined as follows: SiO_2 1.31 wt%, TiO_2 0.19 wt%, Al_2O_3 0.32 wt%, FeO total ($FeO+Fe_2O_3$) 0.91 wt%, MnO 0.14 wt%, MgO 1.32 wt%, CaO 0.26 wt%, Na_2O 0.05 wt%, K_2O 0.08 wt%, P_2O_5 0.01 wt%, LOI 0.07 wt%. Molar element percentage was estimated, and molar element ratio (MER) diagrams were applied to avoid the closure effect (as suggested by e.g. Madeisky & Stanley 1993).

The chemistry of the secondary minerals was obtained on a SEM-JEOL JSM 35 CF upgraded by Point Electronik with a digital control (DISS 5 Electronics) and an energy dispersive X-ray system (EDX) with SDD detector and IDFix software including qualitative, semi-quantitative and quantitative analytical programs at "Eurotest-Control" EAD, Sofia, Bulgaria (manufacturer Micro-analysis-consultants LTD, UK). Analytical conditions: accelerating voltage 20 keV, beam current 20 nA, working distance WD 39mm. The following certified reference materials were used: albite (certified values Na 11.18 %, Al 13.60 %; Si 27.40 %, Ca 0.38 %), wollastonite (Ca 37.10 %, Mg 0.39 %), orthoclase (Si 32.09 %, Al 11.38 %; K 11.63 %; Na 2.37 %; Ba 0.19 %), magnesium oxide (Mg 60.31 %), aluminium oxide (Al 52.93 %), pyrite (Fe 44.52 %, S 55.48 %), titanium (Ti 100 %), strontium fluoride (Sr 69.75 %, F 30.25 %), barium fluoride (Ba 78.33 %, F 21.67 %). Trace elements in biotite were measured by LA-ICP-MS at the Geological Institute of the Bulgarian Academy of Sciences on a Perkin Elmer – ELAN DRC spectrometer with a New Wave UP193FX LA device. The internal standard (SiO_2) was from the microprobe analyses of the respective mineral and NIST 610 and NIST 612 were external standards. The laser system operated at constant 8 Hz pulse rate and laser energy 1.80–2.60 J/cm^2 on the sample surface of 25 to 35 μm spot size.

Results

Spatial distribution and petrography of altered rocks

Mineral assemblages of hydrothermal alteration types based on own spatial and petrographic observations are summarized in Table 1.

The Na–Ca alteration is rarely observed at the deposit, mainly in drill holes from its eastern part (GP-48). The alteration affects quartz-monzodiorite porphyries and granodiorite porphyries. A variety of veins with amphibole (Fig. 4A), amphibole–epidote and albite are formed in granodiorites of the Vezhen pluton, sometimes the veins cross-cut rocks with

Table 1: Types of hydrothermal alteration and mineral associations of the rocks from Elatsite PCD, Abbreviations: GD – Granodiorites from Vezhen pluton, QMDP – Upper Cretaceous quartz-monzodiorite porphyries, GDP – Upper Cretaceous granodiorite porhyries, HFS – hornfelses, Ep – epidote, Px – pyroxene, Amph – amphibole, Prt – prehnite, Pl – plagioclase, Cc – calcite, Chl – chlorite, Py – pyrite, CPy – chalcopyrite, Mo – molybdenite, Mt – magnetite, Hem – hematite, Rut – rutile, Zrn – zircon, Ap – apatite, Bt – biotite, Kfs – potassium feldspar, Tit – titanite, Anh – anhydrite, Ser – sericite (white mica), Qz – quartz, Zeol – zeolites, Adu – adularia, Ft – fluorite, Kaol – kaolinite.

Alteration type	Host rock	Mineral association
Na–Ca alteration	QMDP, GDP	Pl, Amph, Mt, Hem, Rut, Tit, Chl, Ep, Qz
Na–Ca–K-silicate alteration	GDP, QMDP	Bt, Amph, Pl, Kfs±Px, Ep, Prt, Tit, Mt, Ap
K-silicate alteration	GD, QMDP, HFS	Bt, Kfs±Mt, Hem, Anh, Tit, Ap, Zrn, Qz
K-silicate–sericitic alteration	GD, QMDP, HFS	Chl, Ser±Tit, Rut, Py, CPy, Prt
Quartz–sericitic alteration	QMDP, GDP, GD, HFS	Pl, Ser, Qz, Pyr
Propylitic alteration	QMDP, GDP, GD	±Pl, Chl, Ser, Ep, Cc, Zeol, Ap, Py
Quartz–adularia–carbonate alteration	QMDP, GDP, GD, HFS	Qz, Cc, Adu±Chl, Pl, Zeol, Ep, Zrn, Ap, Ft, Ser, Py, Cpy, Prt, etc.
Argillic-like alteration	QMDP, GDP	Kaol, Ser, Qz, ±Cc, Chl, Zeol

previously formed K-silicate alteration (Fig. 5J). The rocks affected by the Na–Ca alteration have pale grey to grey-pink color, usually with well-preserved magmatic texture. The mineral assemblage includes amphibole, plagioclase, magnetite, hematite, rutile, titanite, minor epidote, quartz, and chlorite. The newly formed minerals occur in the groundmass and in veins (Fig. 5A and B), rarely obliterating the primary magmatic texture and minerals. Amphibole is pale green and occurs as infilling veins, as uniformly distributed in the groundmass and as replacing magmatic amphiboles (only at single place). Plagioclase usually forms subhedral, small grains up to few μm, infilling veins or in the groundmass. The Na–Ca alteration has an ambiguous relationship with the K-silicate alteration and unclear relationship with the Na–Ca–K-silicate alteration, expressed by penetration of veins with varying composition or superimposed relations.

The Na–Ca–K-silicate alteration is distributed in drill holes from the east side of the open pit in porphyritic rocks (in granodiorite porphyries and rarely in quartz-monzodiorite porphyries). Veins with amphibole and biotite are present in granodiorites of the Vezhen pluton and in locally in hornfelses from SE and SW parts of the open pit. The rocks affected by the Na–Ca–K-silicate alteration are pale grey to intense grey in color (Fig. 4B). The mineral assemblage of this alteration includes secondary amphibole and secondary biotite, minor potassium feldspar, plagioclase, magnetite, titanite, apatite, minor epidote, prehnite, and pyroxene. The primary magmatic texture is usually well preserved. Newly formed amphibole and biotite typically replace primary magmatic mafic minerals (biotite, amphibole) forming small, subhedral to euhedral crystals (Fig. 5E) and occasionally they occur in groundmass or veins. Due to their imposition biotite and amphibole have an ambiguous relationship (Fig. 5E and F). Potassium feldspar and plagioclase occur in groundmass and rarely replace magmatic minerals. The rocks of the Na–Ca–K-silicate alteration are superimposed by the K-silicate alteration and rarely by the quartz–sericitic alteration.

The K-silicate alteration is abundant at the deposit. It is distributed in all lithological varieties, but with higher intensity it occurs in granodiorites of the Vezhen pluton from the northern and central parts of the open pit (Fig. 4C). The field determination of the alteration is relatively well distinguishable by its macroscopic features – secondary minerals form elongated striations that appear to connect two mafic minerals and form "tails" (Fig. 4D). Veins with secondary biotite occur in hornfelses and in some schists from SE parts of the open pit. The mineral assemblage of the K-silicate alteration includes secondary biotite, potassium feldspar, magnetite, anhydrite, minor hematite, titanite, zircon, apatite, and quartz. Two petrographic varieties are defined: dominated by potassium feldspar and dominated by secondary biotite. The secondary biotite is fine-grained and subhedral, replacing magmatic mafic minerals (mainly amphibole and biotite), uniformly distributed or filling nest and veins (Fig. 5D). The potassium feldspar forms fine-grained subhedral to anhedral grains, occurs as pseudomorphs on primary feldspar and plagioclase and rarely it forms veins with secondary biotite and hematite. Anhydrite is rarely preserved as subhedral to euhedral grains, and it is more common in the variety of the alteration dominated by secondary biotite (Fig. 5C). Rarely, anhydrite veins with biotite and quartz are observed in granodiorites of the Vezhen pluton. Magnetite and hematite usually form anhedral grains or aggregates. Zircons are rare and usually occur with the secondary biotite-dominated variety, as subhedral to euhedral grains. Apatite forms small euhedral grains or clusters around the secondary biotite.

The K-silicate–sericitic alteration is the most widespread alteration at the deposit. Its spatial distribution is related to the previously formed K-silicate and rarely Na–Ca–K-silicate alteration, since the last is not common. The highest intensity is observed in W-NW parts of the deposit in granodiorites of the Vezhen pluton (Fig. 4E). The mineral assemblage includes mainly chlorite, less common sericite, sulfide minerals (chalcopyrite and pyrite), minor rutile, rare titanite and prehnite. The most typical for this alteration are chlorite (Fig. 5G) and sericite (Fig. 5H) replacing secondary biotite of the two earlier alteration types. On macroscopic scale the alteration is distinguished from the K-silicate alteration by the loss of luster of secondary biotite and a matte luster of newly formed chlorite and sericite. The newly formed chlorite has pale green to green color and forms subhedral disseminated flakes. Rutile and titanite typically occur as small anhedral grains in the

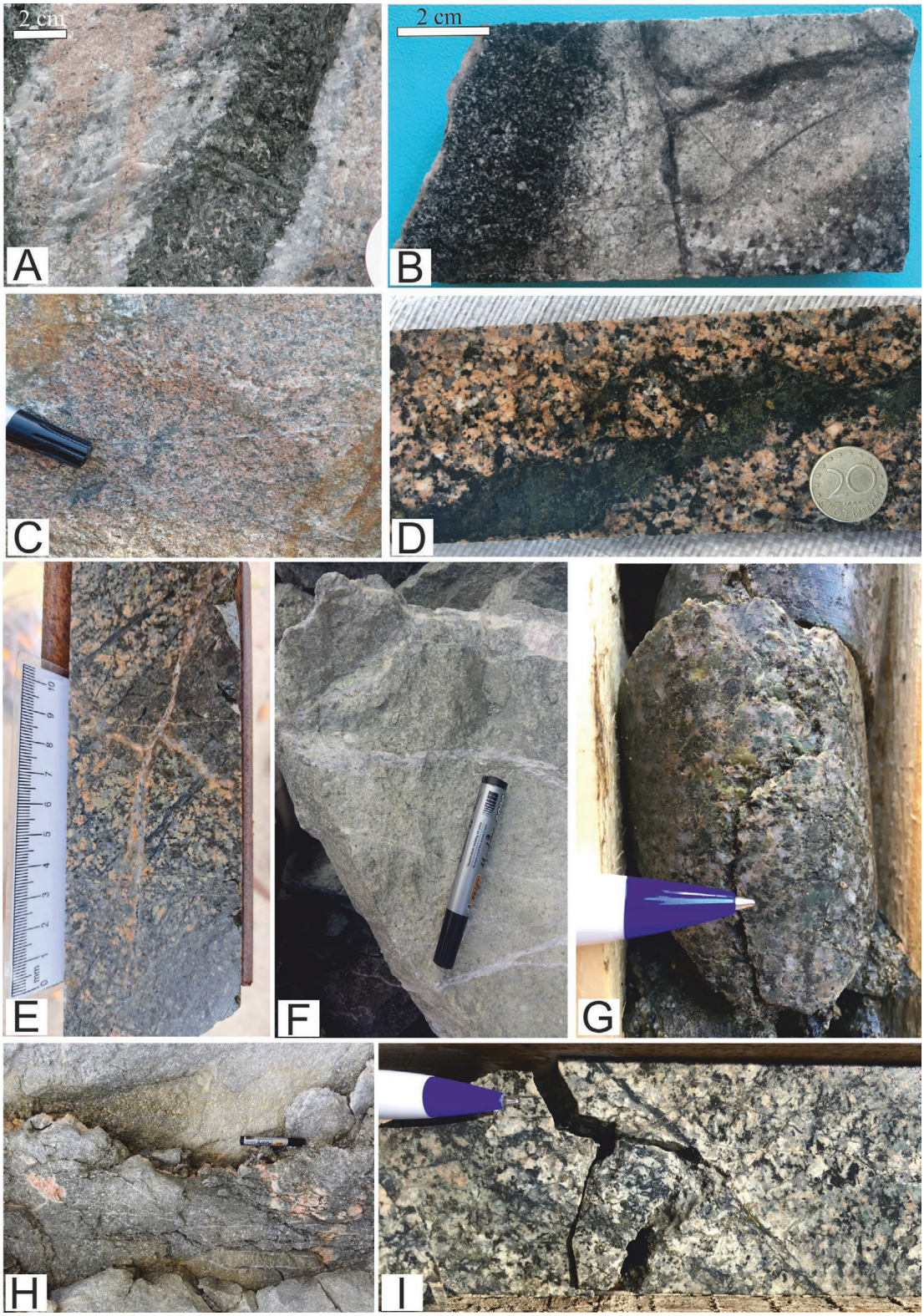

Fig. 4. Macrophotographs of alteration types: **(A)** Amphibole vein of the Na–Ca-alteration, with amphibole grains up to 1 cm long; **(B)** Na–Ca–K-silicate alteration, with amphibole–biotite veins and fine-grained secondary amphibole and biotite in groundmass of a porphyritic rock; **(C)** K-silicate alteration, with biotite–magnetite veins cross-cut by later quartz–sulfide veins; **(D)** secondary biotite forming "tails" and magnetite–chalcopyrite vein with biotite in a rock affected by the K-silicate alteration; **(E)** K-silicate–sericitic alteration superimposed over the K-silicate alteration; **(F)** intensive quartz–sericitic alteration in the porphyritic rocks, cross cut by quartz–pyrite veins; **(G)** propylitic alteration with chlorite and epidote; **(H)** quartz–adularia–carbonate alteration including carbonate nests in a porphyritic rock; **(I)** argillic-like alteration superimposed over K-silicate alteration.

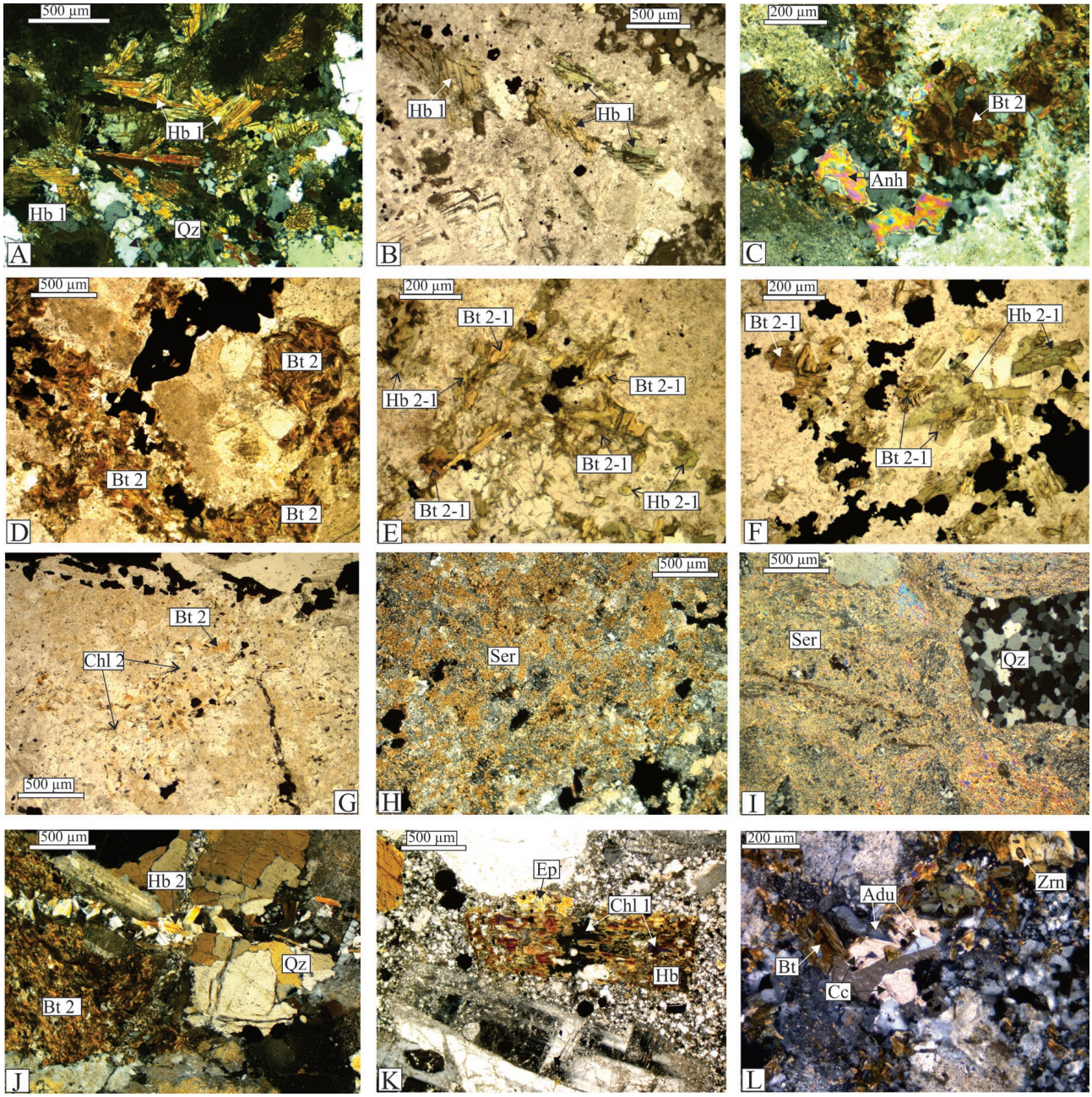

Fig. 5. Microphotographs of alteration minerals: **(A)** and **(B)** Amphiboles from the Na-Ca alteration (×N; ǁN); **(C)** secondary biotite and anhydrite in the K-silicate alteration (×N); **(D)** Fine-grained, subhedral secondary biotite in the K-silicate alteration (×N); **(E)** secondary biotite and amphibole replacing a magmatic mineral (ǁN); **(F)** Secondary biotite and amphibole in the Na–Ca–K-silicate alteration (ǁN); **(G)** chlorite replacing secondary biotite (ǁN); **(H)** sericite replacing secondary biotite (×N); **(I)** sericite and quartz from the quartz–sericitic alteration in a porphyritic rock (×N); **(J)** amphibole veins crosscutting secondary biotite of the K-silicate alteration (×N); **(K)** chlorite and epidote replacing magmatic amphibole (×N); **(L)** Nests of the quartz–adularia–carbonate alteration in a rock affected by the K-silicate–sericitic alteration (×N). Abbreviations: Hb – amphibole, Bt – biotite, Anh – anhydrite, Ser – sericite, Ep – epidote, Chl – chlorite, Adu – adularia, Cc – calcite, Qz – quartz.

periphery of secondary biotite due to its chloritization. Chalcopyrite and pyrite occur as subhedral to euhedral grains.

The quartz–sericite alteration is the third most common alteration at the deposit. It affects mainly porphyritic rocks from the SW part of the deposit (Fig. 4F). The quartz–sericitic alteration is developed in rocks of the Vezhen pluton and in some hornfelses from the SE part where it has a clear structural control. The rocks affected by this alteration have pale grey-green color. The mineral assemblage of quartz–sericite alteration includes quartz, sericite, pyrite, plagioclase, and clay minerals. Usually, the newly formed minerals obliterate primary magmatic feldspar or plagioclase, and the alteration is spreading from the center to the periphery zones of the grains and in the groundmass. With the increase of

intensity of alteration of magmatic mafic minerals the rocks become brighter (Fig. 5I). Plagioclase is fine-grained subhedral to anhedral, usually uniformly distributed in the groundmass and rarely it is replacing magmatic plagioclase. Quartz grains are small, anhedral, usually forming aggregates with sericite. The alteration is superimposed on the K-silicate alteration and overlain by the argillic-like and the quartz–adularia–carbonate alterations, occasionally it is observed as a halo around pyrite and quartz–pyrite veins.

The propylitic alteration is relatively uncommon at the open pit, distributed in the upper SE and some N part of the deposit. Outside the open pit the alteration is well preserved within rocks of the Vezhen pluton and porphyritic rocks. The rocks affected by the propylitic alteration are pale green to rarely intense green with preserved primary texture (Fig. 4G). The mineral assemblage of propylitic alteration includes the formation of chlorite, epidote, plagioclase, carbonates, zeolites, sericite, pyrite, and apatite. Two subtypes of this alteration are determined: chlorite–carbonate and epidote–chlorite. The chlorite–carbonate variety is described in the upper SE part of the mine, whereas the epidote-chlorite variety is preserved in its upper southern part in porphyritic rocks (Fig. 5K). Chlorite is the most common mineral in both varieties. It has an intense green to pale green color, forming subhedral flakes, usually replacing magmatic minerals (typically biotite and amphibole, and rarely pyroxene). Epidote is yellow green, subhedral to rarely euhedral, usually obliterating primary amphibole and biotite. Carbonate occurs in the groundmass or it is replacing plagioclase and feldspars. Plagioclases usually occur in the groundmass as small euhedral grains. Zeolites are rare also in the groundmass or infilling fractures. Zircon is more typical for the epidote–chlorite variety, occurring as small subhedral grains. The propylitic alteration is overlain by the quartz–adularia–carbonate alteration.

The quartz–adularia–carbonate alteration is well preserved at the deposit. It is observed in all lithological varieties (Fig. 4H) and superimposed on all previously formed hydrothermal alteration types. Usually, the alteration is present in nest and stripes (Fig. 5L). It is characterized by the presence of quartz, adularia and variety of carbonate minerals, but chlorite, epidote, plagioclase, sericite, zeolites, sulfides (pyrite and chalcopyrite), prehnite, zircon, apatite, and fluorite are also present. The distribution of these minerals exhibits a distinct asymmetric spatial pattern. In the eastern parts of the deposit adularia dominates, occurring in thin veins with pale pink color, while in the western parts bigger carbonate-dominated veins are present. Adularia is usually represented by its typical pseudorhombic shapes. It forms clear crystals, rarely slightly "clayey", possibly affected by later alteration. Adularia occurs along peripheral parts of the veins or in nests, while calcite chlorite, quartz, zeolites, fluorite, and ore minerals are usually present in their inner parts. Rarely, it replaces primary minerals and occurs in the periphery of magmatic minerals. A variety of carbonate minerals are associated with the alteration: calcite (most common), Mn-calcite, Fe- and Mg-carbonates. Calcite is usually anhedral to subhedral. Quartz is an anhedral and usually forms bigger crystals compared to other minerals in the mineral assemblage. Chlorite is present in nests and veins with carbonate minerals (typically calcite), quartz, adularia, and epidote. It occurs as small, pale green to colorless radial grains. Zeolites are represented by laumontite, stilbite, and chabazite (determined by XRD, Fig. A in the Electronic Supplement). The other minerals are rare and irregularly distributed.

The argillic-like alteration is poorly preserved at the deposit, forming a vein-type alteration with low intensity. It occurs in porphyritic rocks and in rocks of the Vezhen pluton, usually developed around fractures. The alteration is superimposed on the quartz–sericitic alteration in drill holes from the SW part of the deposit, where it rarely overprints the K-silicate alteration (Fig. 4I). The mineral assemblage of the argillic-like alteration includes kaolinite, illite, smectite, carbonate, quartz, sericite, chlorite, and zeolites (Fig. B in the Electronic Supplement). These minerals usually replace primary magmatic minerals (plagioclase and feldspar, and rarely mafic minerals).

Lithogeochemistry

Distribution of major and trace elements in hydrothermal alteration

The data obtained for the hydrothermal alteration of rocks are compared to published data of corresponding unaltered rocks. The data for unaltered granodiorites are published in Kamenov et al. (2002), and for the unalter porphyritic rocks in von Quadt et al. (2002). The new data for major and trace elements content of altered rocks is available in the Electronic Supplement.

One of the main aspects of studies of hydrothermal alteration in porphyry-copper deposits is the selection of immobile elements, such as Ti, Al, and Zr, that are often used to perform the gain-loss analysis, as the elements are described as relatively immobile during the hydrothermal alteration (e.g., Ulrich & Heinrich 2002; Idrus et al. 2009). The correlation coefficient (r) is used to estimate the relative immobility of one element with respect to the other element (MacLean & Kranidiotis 1987). The r for Ti vs. Zr for altered rocks is 0.70 (n=30), so we consider these elements as relatively immobile (as considered by others, e.g., Idrus et al. 2009). The Ti/Zr ratio is used as a benchmark to refer a gain or loss of other elements.

Major element molar percentages are plotted against Ti/Zr ratio with respect to the host rock type. For the K-silicate and the K-silicate–sericitic alterations in granodiorites of the Vezhen pluton a gain of K and loss of Mg, Ca, Na, and Fe occurs (Fig. 6A to D). Loss of Co, Zn, Y, Ba and gain of Rb and Cu is also present (Fig. 6E to L). The increasing contents of K and Rb of the K-silicate alteration correspond to the formation of potassium feldspar and biotite, while the decreasing contents of Ca, Na, Co, Zn, and partly of Fe_{total}, Sr, and Ba are probably related to the destruction of primary minerals (mainly amphibole).

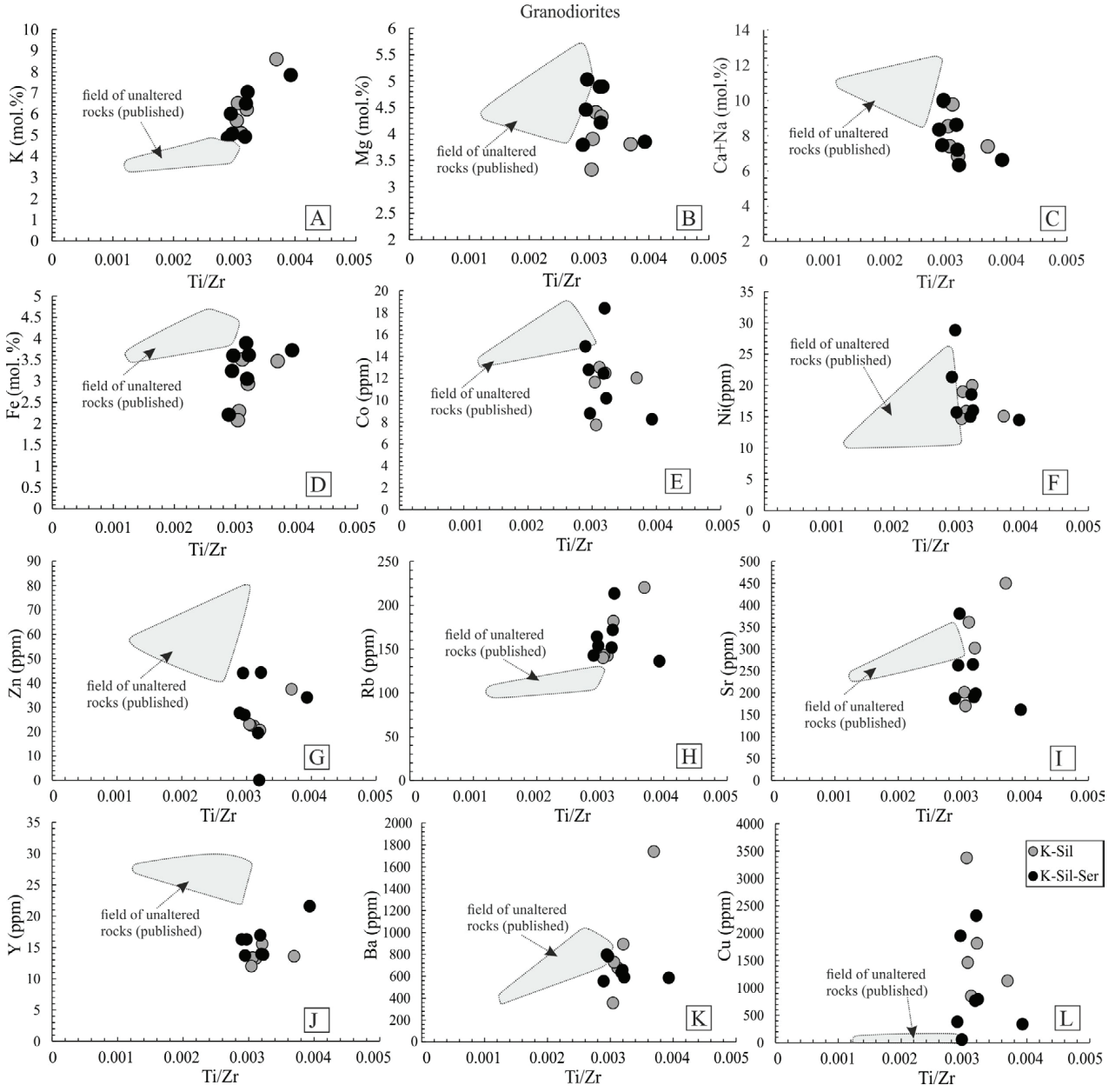

Fig. 6. Diagrams of Ti (mol %) to Zr (ppm) ratio vs. major element (mol%) or trace element (ppm) for different alteration types affecting granodiorites of the Vezhen pluton. Data for unaltered rocks are from Kamenov et al. (2002). Fe total=Fe^2+Fe^3

For porphyries affected by the Na–Ca–K-silicate alteration depletion in Fe, slight depletion in Ca and increasing K (Fig. 7A to D) are probably related to the formation of secondary biotite and K-feldspar. The depletion in Fe_{total}, Ca, Co, Ni, S, and Ba is probably related to the destruction of mafic minerals (amphibole and biotite) (Fig. 7E to L), while increasing Cu is related to the formation of chalcopyrite. In the Na–Ca alteration a slight increase in K, Mg, Ca, and Na probably corresponds to the formation of amphibole (typical for this alteration) and the increased contents of Na correspond to the formation of albite, nevertheless the values are close to data of unaltered rocks. This alteration type is also characterized by a loss of Co, Ni, Zn, Y and gain of Ba, Sr, and Cu. In the K-silicate–sericitic alteration depletion in Ca, Na, slight depletion in Fe, Co, Bi, and Ba and slight increase in Mg and K probably correspond to the formation of chlorite, while the increasing values for K correspond to the formation of sericite. Gain of Cu reflects the formation of chalcopyrite (Fig. 7L). For the quartz–sericitic alteration depletion in Mg, Ca, Na, Ni, Zn, Sr, and Y is present. The depletion in Na and partly in Ca and the increase in K and Rb corresponds to the destruction of feldspar and formation of sericite, while the depletion in Mg, partly Ca, Ni, Zn, Sr results from the alteration of primary mafic minerals. The gain of copper corresponds to the formation of chalcopyrite. For propylitic alteration no significant geochemical changes are determined,

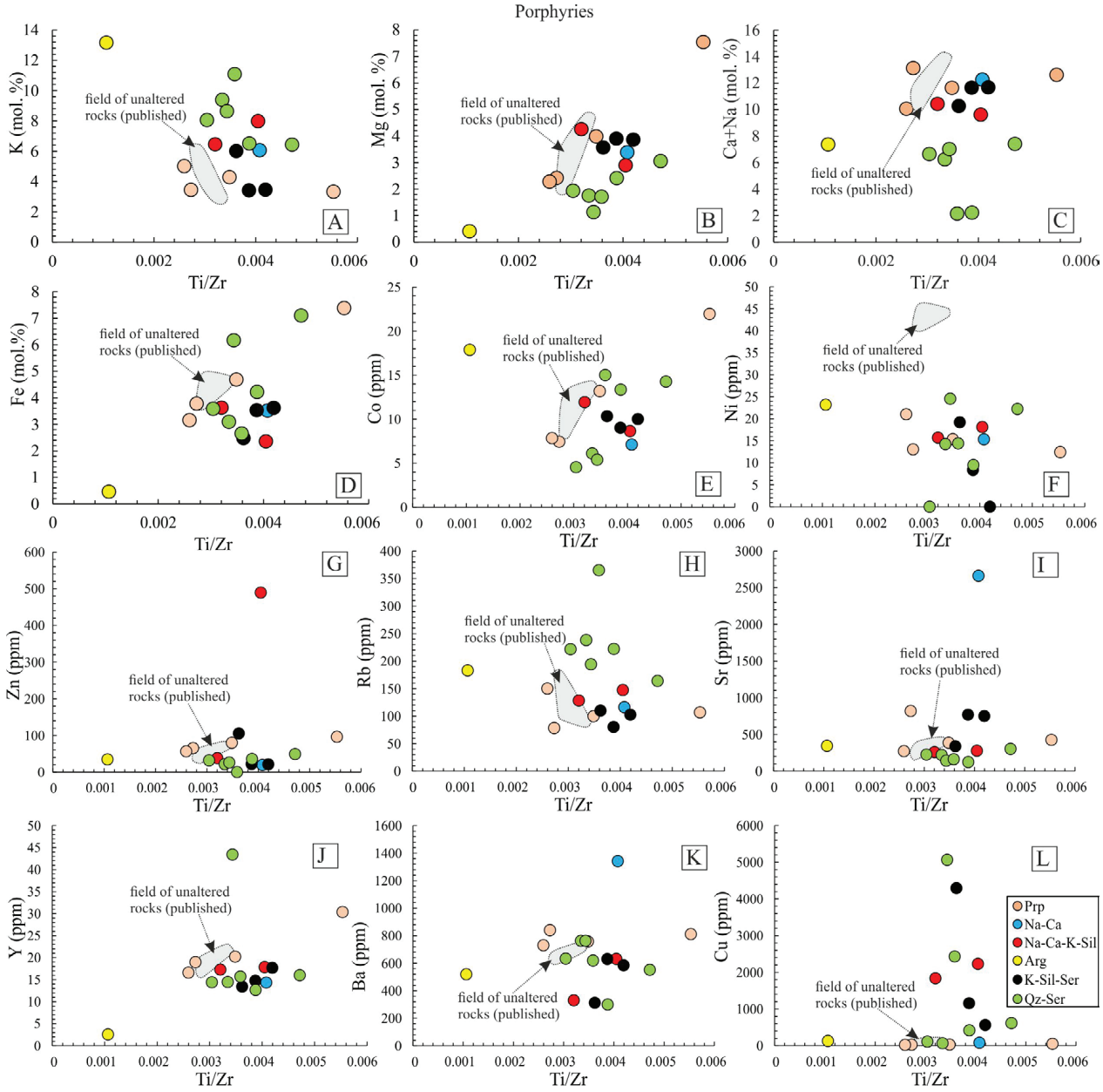

Fig. 7. Diagrams of Ti (mol%) Zr (ppm) vs. major element (mol%) or trace element (ppm) for different alteration types affecting Cretaceous porphyries. Data for unaltered rocks from von Quadt et al. (2002). Fe total=Fe^2+Fe^3

except at one sample with gain of Mg and Fe, probably corresponding to the domination of chlorite and formation of pyrite in the mineral assemblage (Fig. 5K). For the argillic-like alteration depletion in Fe, Mg, Ca, and Na is related to the destruction of plagioclase and primary mafic minerals and increase in K and Rb corresponds to the formation of kaolinite and white micas.

Molar element ratio diagrams

Molar element ratio diagrams (MER) are used to help graphically present the metasomatism of altered rocks (e.g., Madeisky & Stanley 1993; Byrne et al. 2020; Siani & Lentz 2022), and alkali/alumina diagrams are used to improve the comparison with a corresponding mineral assemblage (e.g., Davies & Whitehead 2010; Siani & Lentz 2022).

The Al/Ti vs. Mg/K, 2Ca+Na+K/Al vs. Al/Ti, and Mg/Al vs. K/Al diagrams excellently distinguish unaltered granodiorites form the K-silicate and K-silicate–sericitic types of alteration due to the gain of K, loss of Mg, Ca, and Na, and by higher Al/Ti ratio of altered rocks (Fig. 8A, B, C). The quartz–sericitic alteration is well distinguished from unaltered porphyries and relatively well from the K-silicate–sericitic alteration due to the gain of K and loss of Ca, Na (Fig. 8D and E). Na–Ca–K-silicate alteration is plotted close to the unaltered rocks field due to the addition of K and loss of Ca,

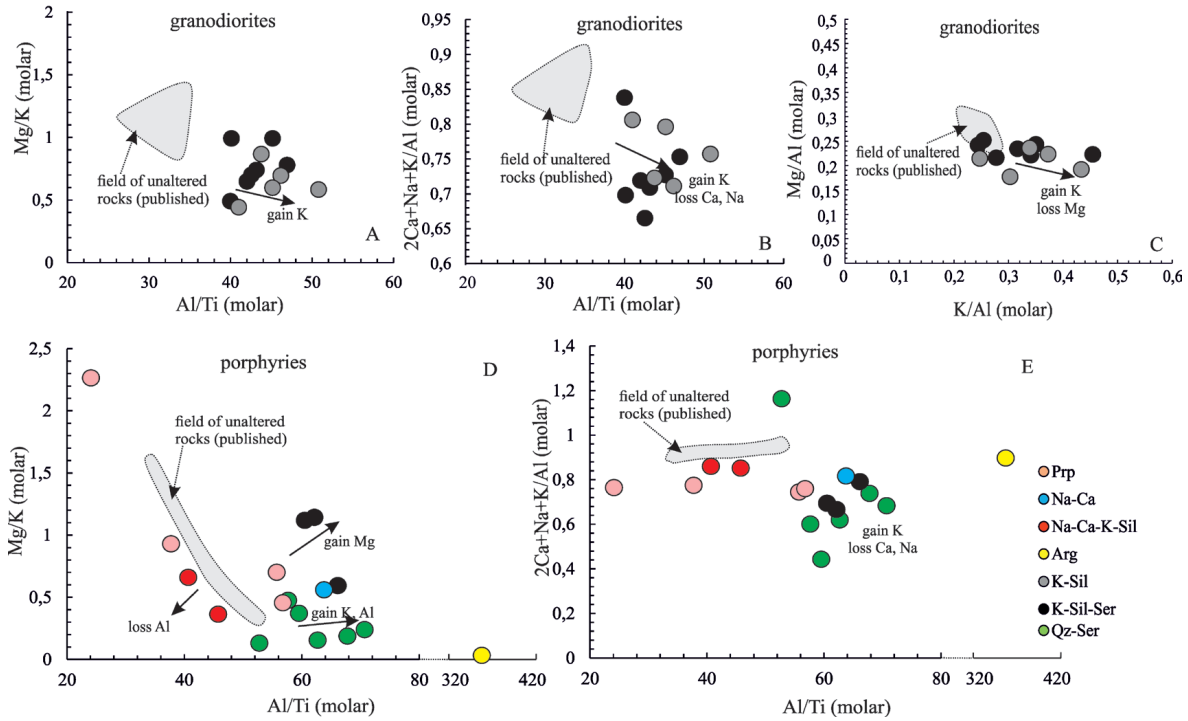

Fig. 8. Molar element ratio diagrams for variety of hydrothermal alteration types affecting granodiorites of the Vezhen pluton (**A**, **B** and **C**) and affecting Cretaceous porphyries (**D** and **E**). Data for unaltered rocks from Kamenov et al. (2002) and von Quadt et al. (2002).

with the formation of secondary biotite and amphibole. The plotting of the argillic-like alteration data far to the right side of the diagrams results from the addition of K and Al due to the formation of kaolinite and clay minerals (Fig. B in the Electronic Supplement).

Molar K/Al vs. Na/Al diagram (Fig. 9) indicates that all samples below the plagioclase-potassium feldspar (biotite) line and left side of the albite-muscovite line are depleted in Na and enriched in K, which corresponds to the samples affected by the K-silicate and the K-silicate–sericitic alterations with mineral association of biotite, potassium feldspar, chlorites, plagioclase, and muscovite (sericite). The quartz–sericitic alteration plots in strongly K-enriched part of the diagram, related to the feldspar destruction and sericite formation. The Na–Ca–K-silicate alteration samples are plotted to the plagioclase–potassium feldspar (biotite) line, which correlates excellently with petrographic observations. The Na–Ca alteration shows no significant deviation from unaltered samples, as this alteration is related dominantly to a gain of Ca. A similar result is visible for the propylitic alteration. The K/Al vs. Na/Al diagram, however, is not suitable for the argillic-like sample, as it plots on the right side of the plagioclase–potassium feldspar (biotite) line, which corresponds to the increase in Al with the formation of kaolinite.

Distribution of Rare Earth Elements

On the chondrite normalized distribution pattern for REEs in the K-silicate alteration and the K-silicate–sericitic alteration in granodiorites of the Vezhen pluton depletion of all elements is present (Fig. 10A). For the K-silicate alteration with La_N/Yb_N 6.19–13.19 the ∑REE is 94.37–139.15 (average ∑REE=108.15), for the K-silicate-sericite alteration the ∑REE is 94.84–148.05 (average ∑REE=117.85) which are lower values than of unaltered granodiorites with La_N/Yb_N 3.39–12.23 (∑REE=481.42–570.64, average ∑REE=533.03). The close values for ∑REE of the K-silicate and the K-silicate–sericite alterations are related to the varying intensity of alteration and the replacement of secondary biotite by chlorite and sericite. The decreasing values for all REEs are probably related to their incorporation into the fluids (e.g., Siani & Lentz 2022).

For the Na–Ca, Na–Ca–K-silicate and argillic-like alteration types a depletion is shown for all REEs (Fig. 10B). For the Na–Ca alteration with La_N/Yb_N 6.68 the ∑REE is 111.02, for the Na–Ca–K-silicate alteration with La_N/Yb_N 4.62–7.87 the ∑REE is 85.68–121.46 and the lowest values are for the argillic-like alteration (∑REE=20.12).

The values for ∑REE in the propylitic alteration are higher than for unaltered rocks (Fig. 10B). In quartz-monozdiorite porphyries with La_N/Yb_N 6.63 the ∑REE is 148.76 and in granodiorite porphyries with La_N/Yb_N 7.73–17.63 the ∑REE is 136.96–172.25 (average ∑REE=154.84).

For the quartz–sericitic alteration in quartz-monzodiorite porphyries with La_N/Yb_N 5.93–10.94 the ∑REE is 88.46–130.09 (average ∑REE=107.49), just one sample showed higher values (∑REE=190.80 and La_N/Yb_N=4.86) with carbonate included into the mineral assemblage. In granodiorite porphyries with La_N/Yb_N 12.19 the ∑REE is 134.57.

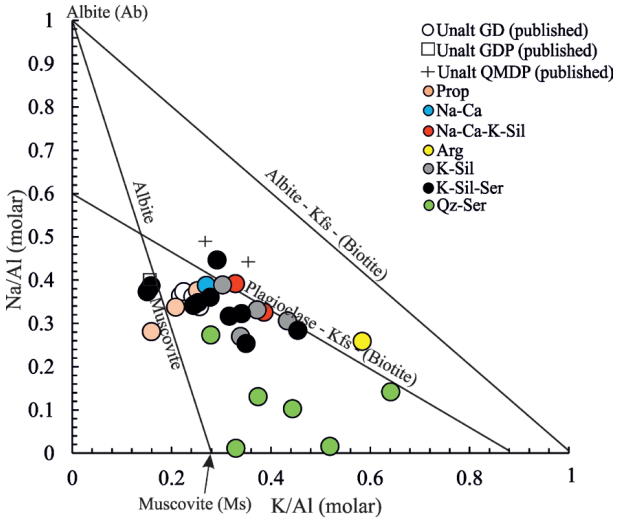

Fig. 9. Molar element ratio plot Na/Al vs. K/Al for various hydrothermal alteration types and unaltered rocks. Mineral control lines are plotted based on the stoichiometry of the corresponding minerals (after Davies & Whitehead 2010). GD – unaltered granodiorites from Vezhen pluton (Kamenov et al. 2002); GDP – unaltered granodiorite porphyries (von Quadt et al. 2002); QMDP – unaltered quartz-monzodiorite porphyries (von Quadt et al. 2002).

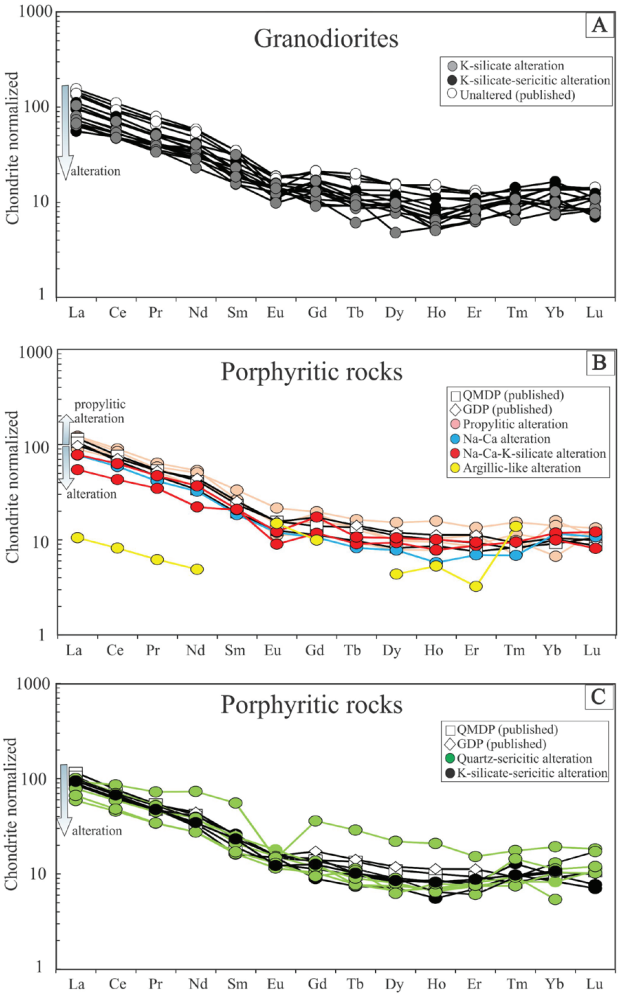

Fig. 10. Rare earth elements distribution patterns for hydrothermal alteration types and unaltered rocks from the Elatsite deposit. Data for the unaltered granodiorites (GDP) are from Kamenov et al. (2002) and for unaltered porphyries (QMDP) from von Quadt et al. (2002). Normalization of REEs was made after Boynton (1984).

For the K-silicate–sericite alteration in quartz-monzodiorite porphyries with La_N/Yb_N 10.68 the ∑REE is 116.53 and in granodiorite porphyries with La_N/Yb_N 8.86–8.87 the ∑REE is 124.38–127.13, which are values lower than those of unaltered rocks (Fig. 10C).

In summary, the depletion in ∑REE is present for all alteration types except the propylitic alteration and the quartz–sericitic alteration with carbonates.

Mineral chemistry

Biotite

Biotite is one of the most common hydrothermal minerals at the Elatsite deposit. Its occurrence is related to the formation of the K-silicate alteration (biotite marked as Bt 2) and the Na–Ca–K-silicate alteration (biotite marked as Bt 2-1). In the two alteration types biotite is fine-grained with pale brown color, at some places replaced by chlorite or sericite from the K-silicate–sericitic alteration. The Mg* ratio (Mg/Mg+Fe) in Bt 2 varies in range 0.70–0.82 and lower Fe ratio than Bt 2-1 (Fig. 11A). Bt 2-1 has Mg* ratio in range 0.62–0.68 (Table 2). The comparison with magmatic biotite from granodiorites of the Vezhen pluton (Bt 1) reveals Mg* ratio between 0.56–0.64 for Bt 1, which is lower than Bt 2 and close to the value for Bt 2-1. Higher contents for Ti and Ba in Bt 1 than Bt 2 were determined. Using the Ti-in-biotite thermometer (Henry et al. 2005) average temperatures of formation are about 720 °C for Bt 2-1 and 709 °C for Bt 2.

Amphibole

The presence of hydrothermal amphiboles is related to the formation of the Na–Ca alteration (amphibole marked as Hb 2) and the Na–Ca–K-silicate alteration (Hb 2-1). Hb 2 and Hb 2-1 belong to the actinolite-tremolite to magnesio-hornblende series and Hb 2 in monomineral amphibole veins belongs to the actinolite-tremolite series to edenite (Fig. 11B). A comparison between the secondary amphibole and the magmatic amphibole from porphyritic rocks reveals a lower Mg* ratio and lower Ti contents for Hb 1 than for Hb 2 and Hb 2-1. A higher Ca and Al contents are in Hb 1 than in Hb 2 and Hb 2-1 (Table 3).

Plagioclase

The occurrence of secondary plagioclase is related to the formation of the propylitic, quartz–sericitic, Na–Ca and Na–Ca–K-silicate alterations. In plagioclase from the Na–Ca–K-silicate alteration the Ab component varies in range

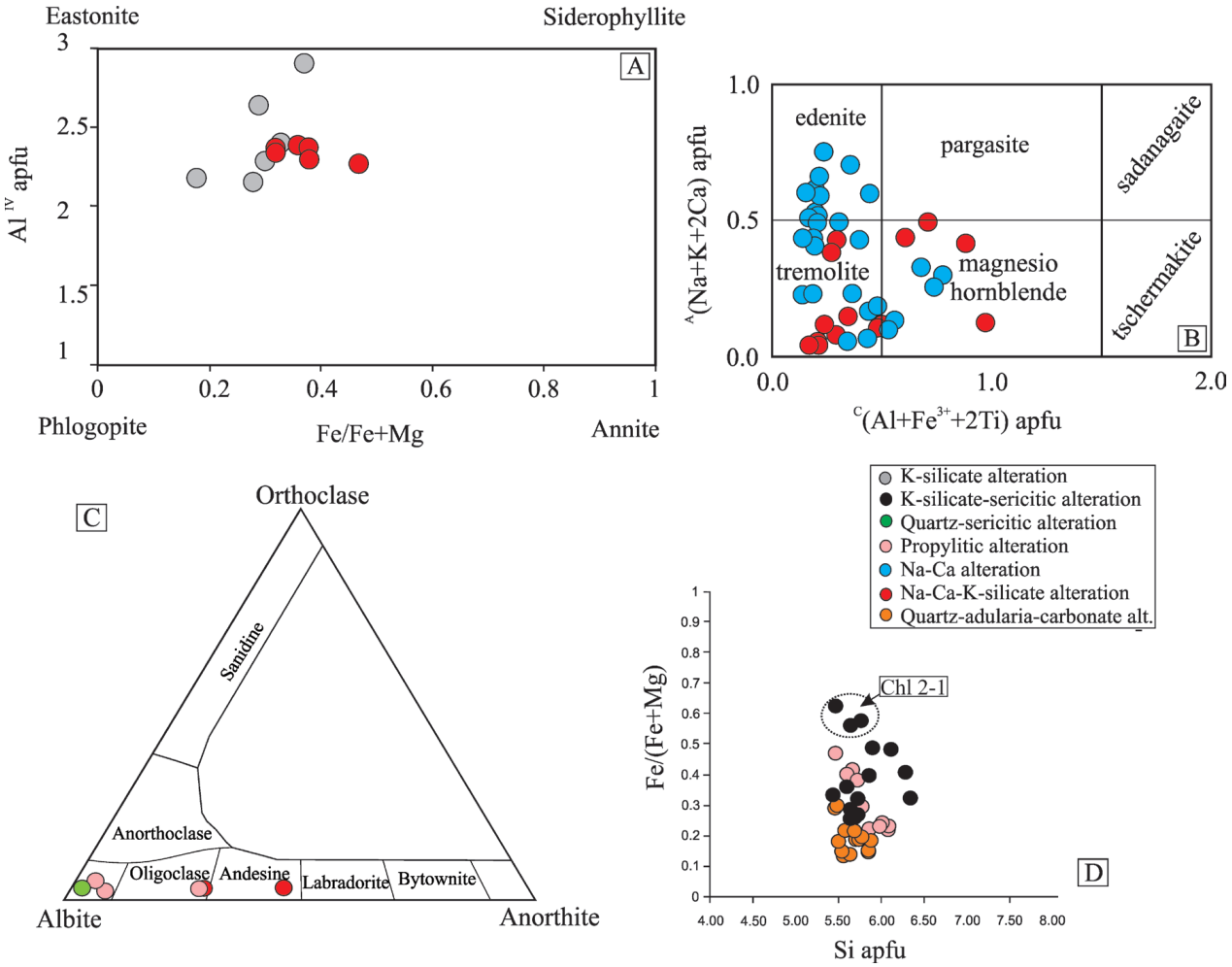

Fig. 11. (A) Classification diagram for secondary biotite (after Deer et al. 1992); **(B)** Classification diagram for secondary amphibole (after Hawthorne et al. 2012); **(C)** Classification diagram for secondary plagioclase; **(D)** Composition of chlorites; Chl 2-1 – chlorite from the K-silicate-sericitic alteration replacing biotite Bt 2-1.

52.12–69.41 and it is described as oligoclase to andesine (Fig. 11C). Plagioclase from the quartz–sericitic alteration occurs as small, subhedral grains (up to few μm), while only one analysis of plagioclase identified albite with the Ab component 94.50 (Table 4). Plagioclase from the propylitic alteration occurs in groundmass, usually with carbonate minerals (such as calcite), identified as albite (with Ab component 90.10–91.44).

Chlorite

Chlorite is the most common hydrothermal mineral at the Elatsite deposit. Its occurrence is related to the formation of the propylitic (chlorite marked as Chl 1), K-silicate–sericitic (Chl 2, Chl 2-1), quartz–adularia–carbonate alterations (Chl 3). All analyzed chlorites belong to the clinochlorite–chamosite series (Wiewiora & Weiss 1990, Fig. 11D) and their chemistry is strongly dependent on the replaced secondary altered mineral and its chemistry (Georgieva & Nedialkov 2021). Chl 1 has Fe* ratio 0.23–0.49, while the Fe* ratio is higher for Chl 1 replacing magmatic amphibole rather the Chl 1 developed on pyroxene (Fe* ratio 0.38–0.49) (Table 5). Chl 2 is one of the dominant minerals in the K-silicate–sericitic alteration where it replaces Bt 2 and Bt 2-1. Chl 2 that replaces Bt 2 has a lower Fe* ratio than Chl 2-1 replacing Bt 2-1. Chl 3 has a varying Fe* ratio 0.15–0.30. The temperature of formation of hydrothermal chlorites is estimated using the thermometer of Kranidiotis & MacLean (1987): Chl 1 ~175–318 °C, Chl 2 ~181–310 °C, Chl 3 ~248–304 °C.

Discussion

Features of the magmatic-hydrothermal system of the Elatsite deposit

One of the main features of the magmatic system at Elatsite is its pulse nature. Two significant pulses are described: first related to the emplacement of quartz-monzodiorite porphyries and second with the granodiorite porphyries (e.g., von Quadt

Table 2: Representative microanalyses and calculated formulae (on the basis of 22 O) of secondary biotite from K-silicate and Na–Ca–K-silicate alteration and for magmatic biotite. The main oxides in wt% and trace elements in ppm. FeO* total iron as FeO; Fe*=Fe/Fe+Mg; Mg*=Mg/Mg+Fe; bdl: below detection limit.

	K-silicate alt.			Na–Ca–K-silicate alt.				Magmatic		
SiO_2	38.86	40.24	39.74	35.36	39.60	38.72	39.66	35.55	36.66	38.66
TiO_2	2.40	2.89	2.07	2.97	3.10	2.78	3.07	3.74	3.13	3.49
Al_2O_3	15.16	13.67	13.88	13.24	14.50	14.62	14.18	15.40	14.63	14.81
Cr_2O_3	0.12	0.09	0.17	0.00	0.00	0.00	0.00	0.19	0.11	0.11
FeO*	12.37	11.97	7.63	17.35	13.34	14.84	13.44	17.26	14.30	14.47
MnO	0.05	0.05	0.07	0.23	0.14	0.15	0.14	0.27	0.23	0.25
MgO	16.32	17.36	20.07	15.93	16.19	15.03	15.91	12.50	14.19	13.48
CaO	0.08	0.11	0.15	0.19	0.05	0.16	0.00	0.30	0.35	0.23
Na_2O	0.38	0.36	0.63	0.47	0.11	0.22	0.00	0.36	1.03	0.37
K_2O	9.43	8.99	9.11	9.04	9.26	8.75	9.46	9.13	9.45	9.17
F	0.00	0.00	1.36	0.00	0.00	0.58	0.40	0.00	0.00	0.00
Cl	0.35	0.35	0.46	0.27	0.14	0.23	0.10	0.62	0.76	0.38
Total	95.52	96.08	95.34	95.05	96.43	96.08	96.36	95.32	94.84	95.42
Si	5.72	5.85	5.82	5.37	5.63	5.62	5.67	5.43	5.56	5.75
Al ^{iv}	2.28	2.15	2.18	2.37	2.37	2.38	2.33	2.57	2.44	2.25
Al ^{vi}	0.35	0.20	0.21	0.00	0.07	0.12	0.06	0.20	0.18	0.35
Ti	0.27	0.32	0.23	0.34	0.33	0.30	0.33	0.43	0.36	0.39
Cr	0.01	0.01	0.02	0.00	0.00	0.00	0.00	0.02	0.01	0.01
Fe	1.52	1.46	0.93	2.20	1.59	1.80	1.61	2.20	1.81	1.80
Mn	0.01	0.01	0.01	0.03	0.02	0.02	0.02	0.03	0.03	0.03
Mg	3.58	3.76	4.38	3.60	3.43	3.25	3.39	2.85	3.21	2.99
Ca	0.01	0.02	0.02	0.03	0.01	0.02	0.00	0.05	0.06	0.04
Na	0.11	0.10	0.18	0.14	0.03	0.06	0.00	0.11	0.30	0.11
K	1.77	1.67	1.70	1.75	1.68	1.62	1.73	1.78	1.83	1.74
OH	3.91	3.91	3.26	3.93	3.97	3.68	3.79	3.84	3.80	3.90
F	0.00	0.00	0.63	0.00	0.00	0.27	0.18	0.00	0.00	0.00
Cl	0.09	0.09	0.11	0.07	0.03	0.06	0.02	0.16	0.20	0.10
Total	19.62	19.53	19.68	19.83	19.15	19.21	19.14	19.67	19.78	19.46
Fe*	0.30	0.28	0.18	0.38	0.32	0.36	0.32	0.44	0.36	0.38
Mg*	0.70	0.72	0.82	0.62	0.68	0.64	0.68	0.56	0.64	0.62
V	599.77	734.34	660.21	334.19	820.53			777.11	723.27	
Cr	432.30	492.04	457.97	bdl	84.97			121.07	84.29	
Co	23.09	20.72	18.85	6.16	35.85			20.25	17.95	
Ni	22.84	177.65	164.03	42.49	bdl			bdl	30.71	
Zn	106.53	74.56	66.03	22.70	81.67			133.94	127.45	
Rb	660.82	955.11	857.41	80.09	378.10			561.82	463.49	
Sr	5.60	13.37	11.58	193.71	52.71			9.97	7.88	
Y	0.53	2.59	2.46	2.03	5.33			0.41	1.57	
Ba	293.55	105.88	93.91	59.78	420.04			2290.61	4133.52	
Pb	1.38	2.43	2.28	1.74	1.83			1.32	bdl	
Th	0.20	1.29	1.13	0.18	0.35			0.08	0.25	
U	0.59	2.66	2.56	0.88	0.92			0.13	0.74	

et al. 2002; Ivanov et al. 2014; Peytcheva et al. 2017a, b). The age determinations of the Cretaceous rocks suggest <0.3 Ma discontinuity between the two magmatic pulses (Peytcheva et al. 2017a, b).

Another feature of the magmatic-hydrothermal system is the formation of magmatic-hydrothermal breccias. Formation of magmatic-hydrothermal breccias is related to an explosive release of magmatic fluids (Burnham 1985) from a porphyritic dome. In the Elatsite deposit this type of breccias occur with the impulse of quartz-monzodiorite porphyries, granodiorite porphyries and quartz-syenite porphyries in the upper contacts of the magmatic bodies in an almost subvertical position (Hadzhieva 2009; Nedialkov et al. 2012; Ivanov et al. 2014). The release of the magmatic fluids from the magmatic body is a pulsive process related to the fluid saturation of the magma during its cooling (Burnham 1979). For Elatsite this means that at least three magmatic-hydrothermal pulses of fluids have been released from the dome, probably with the same time discontinuity as that of the magmatic events (about 0.3 Ma). This suggests that the magmatic-hydrothermal system of the deposit also has a pulsating nature due to the pulsating nature of the Upper Cretaceous magmatic activity.

During the entire period of the Upper Cretaceous magmatic activity (magma evolution, various magmatic pulses, magma

emplacement and cooling), the magma chamber represented a heat source that probably mobilized deeply buried fluids of external origin – sedimentary, metamorphic, deeply penetrated meteoric. The external fluids were circulating in proximal parts of the magmatic center and a fluid-rock interaction probably was a source of components for hydrothermal fluids. The process was relatively constant, with different intensity depending on the depth and sustention of the magmatic center and is not related to the impulse magmatic implementation.

Geochemical behavior of elements and origin of hydrothermal alteration

The manifestation of the Na–Ca alteration is limited to only a few occurrences in the eastern side of the deposit. Some features of the alteration are related to its formation in an environment with a high fO_2 (considering the presence of magnetite in the mineral assemblage), with a high CO_2 potential and pressures between 0.59 and 2.15 kbar (Georgieva et al. 2019).

Table 3: Representative microanalyses of secondary amphibole (on the basis of 23 O) from Na–Ca alteration and Na–Ca–K-silicate alteration and magmatic amphibole from the unaltered porphrtic rocks. The main oxides in wt%. FeO* total iron as FeO; Fe*=Fe/Fe+Mg; Mg*=Mg/Mg+Fe.

	Na–Ca alt.					Na–Ca–K-silicate alt.						Magmatic			
SiO_2	49.96	50.10	51.56	53.85	52.54	54.01	55.95	54.84	54.07	55.17	55.82	45.03	47.07	45.44	46.02
TiO_2	0.85	0.99	0.46	0.00	0.32	0.16	0.00	0.15	0.26	0.00	0.13	1.02	0.84	1.06	1.07
Al_2O_3	6.36	6.70	4.98	3.77	5.16	3.66	1.91	2.91	4.11	2.12	2.27	9.06	9.38	9.77	10.34
Cr_2O_3	0.00	0.00	0.06	0.00	0.00	0.05	0.06	0.00	0.00	0.00	0.00	0.00	0.00	0.00	0.00
FeO	11.66	11.25	9.36	12.11	11.12	9.22	7.88	8.30	9.48	11.43	7.18	17.32	16.53	15.45	15.40
MnO	0.58	0.44	0.43	0.18	0.11	0.24	0.21	0.22	0.10	0.27	0.26	0.40	0.38	0.46	0.48
MgO	14.93	15.30	18.17	16.86	16.61	17.60	19.25	18.17	17.61	16.18	19.59	11.86	12.37	14.28	14.01
CaO	11.20	10.95	10.08	10.55	11.33	11.54	11.44	11.62	11.53	11.99	11.43	11.11	10.47	10.52	10.18
Na_2O	1.50	1.55	1.69	0.28	0.67	0.97	0.48	1.12	0.82	0.39	0.72	1.14	0.00	0.00	0.00
K_2O	0.63	0.61	0.45	0.20	0.36	0.41	0.21	0.26	0.30	0.22	0.25	0.65	0.66	0.61	0.68
Cl	0.23	0.11	0.17	0.08	0.04	0.07	0.08	0.24	0.04	0.09	0.05	0.00	0.00	0.00	0.00
Total	97.90	98.00	97.41	97.88	98.26	97.93	97.47	97.83	98.32	97.86	97.70	97.59	97.70	97.59	98.18
Si	7.20	7.17	7.29	7.66	7.43	7.60	7.84	7.72	7.58	7.85	7.79	6.64	6.88	6.58	6.63
Al	0.80	0.83	0.71	0.34	0.57	0.40	0.16	0.28	0.42	0.15	0.21	1.36	1.12	1.42	1.37
Ti	0.00	0.00	0.00	0.00	0.00	0.00	0.00	0.00	0.00	0.00	0.00	0.00	0.00	0.00	0.00
T	8.00	8.00	8.00	8.00	8.00	8.00	8.00	8.00	8.00	8.00	8.00	8.00	8.00	8.00	8.00
Ti	0.09	0.11	0.05	0.00	0.03	0.02	0.00	0.02	0.03	0.00	0.01	0.11	0.09	0.12	0.12
Al	0.28	0.30	0.12	0.29	0.30	0.21	0.16	0.20	0.26	0.21	0.17	0.21	0.50	0.25	0.39
Cr	0.00	0.00	0.01	0.00	0.00	0.01	0.01	0.00	0.00	0.00	0.00	0.00	0.00	0.00	0.00
Mn^{3+}	0.00	0.00	0.00	0.00	0.00	0.00	0.00	0.00	0.00	0.00	0.00	0.00	0.00	0.00	0.00
Fe^{3+}	0.21	0.26	0.52	0.05	0.19	0.26	0.05	0.11	0.16	0.00	0.10	0.74	0.31	0.83	0.62
Mn^{2+}	0.01	0.00	0.00	0.00	0.00	0.00	0.00	0.00	0.00	0.00	0.00	0.00	0.00	0.00	0.00
Fe^{2+}	1.19	1.06	0.48	1.08	0.97	0.82	0.76	0.86	0.87	1.35	0.64	1.33	1.40	0.72	0.86
Mg	3.21	3.27	3.83	3.58	3.50	3.69	4.02	3.81	3.68	3.43	4.08	2.61	2.70	3.08	3.01
Li	0.00	0.00	0.00	0.00	0.00	0.00	0.00	0.00	0.00	0.00	0.00	0.00	0.00	0.00	0.00
C	5.00	5.00	5.00	5.00	5.00	5.00	5.00	5.00	5.00	5.00	5.00	5.00	5.00	5.00	5.00
Mn^{2+}	0.06	0.05	0.05	0.02	0.01	0.03	0.02	0.03	0.01	0.03	0.03	0.05	0.05	0.06	0.06
Fe^{2+}	0.00	0.02	0.11	0.31	0.15	0.01	0.11	0.01	0.09	0.00	0.10	0.07	0.31	0.31	0.37
Mg	0.00	0.00	0.00	0.00	0.00	0.00	0.00	0.00	0.00	0.00	0.00	0.00	0.00	0.00	0.00
Li	0.00	0.00	0.00	0.00	0.00	0.00	0.00	0.00	0.00	0.00	0.00	0.00	0.00	0.00	0.00
Ca	1.73	1.68	1.53	1.61	1.72	1.74	1.72	1.75	1.73	1.83	1.71	1.76	1.64	1.63	1.57
Sr	0.00	0.00	0.03	0.00	0.00	0.00	0.03	0.01	0.00	0.03	0.00	0.00	0.00	0.00	0.00
Na	0.21	0.25	0.29	0.06	0.12	0.22	0.11	0.21	0.17	0.11	0.16	0.13	0.00	0.00	0.00
B	2.00	2.00	2.00	2.00	2.00	2.00	2.00	2.00	2.00	2.00	2.00	2.00	2.00	2.00	2.00
Ca	0.00	0.00	0.00	0.00	0.00	0.00	0.00	0.00	0.00	0.00	0.00	0.00	0.00	0.00	0.00
Li	0.00	0.00	0.00	0.00	0.00	0.00	0.00	0.00	0.00	0.00	0.00	0.00	0.00	0.00	0.00
Na	0.21	0.18	0.18	0.02	0.06	0.04	0.02	0.10	0.05	0.00	0.03	0.20	0.00	0.00	0.00
Pb	0.00	0.00	0.00	0.00	0.00	0.00	0.00	0.00	0.00	0.00	0.00	0.00	0.00	0.00	0.00
K	0.12	0.11	0.08	0.04	0.06	0.07	0.04	0.05	0.05	0.04	0.04	0.12	0.12	0.11	0.13
A	0.33	0.30	0.26	0.05	0.13	0.12	0.05	0.14	0.11	0.04	0.08	0.32	0.12	0.11	0.13
W 2apfu	2.00	2.00	2.00	2.00	2.00	2.00	2.00	2.00	2.00	2.00	2.00	2.00	2.00	2.00	2.00
OH	1.94	1.97	1.96	1.98	1.99	1.98	1.98	1.94	1.99	1.98	1.99	2.00	2.00	2.00	2.00
Cl	0.06	0.03	0.04	0.02	0.01	0.02	0.02	0.06	0.01	0.02	0.01				
Mg*	0.70	0.71	0.78	0.71	0.73	0.77	0.81	0.80	0.77	0.72	0.83	0.55	0.57	0.62	0.62
Fe*	0.30	0.29	0.22	0.29	0.27	0.23	0.19	0.20	0.23	0.28	0.17	0.45	0.43	0.38	0.38

Table 4: Representative microanalyses and calculated formula (on the basis of 8 O) of secondary plagioclase from Na–Ca–K-silicate alteration, propylitic alteration and quartz–sericitic alteration. Main oxides in wt%; FeO* total iron as FeO.

	Na–Ca–K-silicate alt.		Propylitic alt.		Qz-Ser alt.
SiO_2	59.47	55.58	62.86	63.02	61.48
Al_2O_3	24.93	27.60	21.29	21.26	20.89
FeO*	0.16	0.08	0.14	0.19	0.17
MnO	0.09	0.00	0.13	0.13	0.12
MgO	0.46	0.39	0.66	0.66	1.21
CaO	5.82	9.19	1.66	0.85	0.56
Na_2O	8.06	5.93	10.98	10.92	13.34
K_2O	0.51	0.56	0.44	0.84	0.71
BaO	0.00	0.00	0.54	0.41	0.55
Total	99.50	99.33	98.70	98.28	99.03
Si	2.68	2.53	2.85	2.86	2.82
Al	1.32	1.48	1.14	1.14	1.13
Fe^{ii}	0.01	0.00	0.01	0.01	0.01
Ca	0.28	0.45	0.08	0.04	0.03
Na	0.70	0.52	0.97	0.96	1.19
K	0.03	0.03	0.03	0.05	0.04
Ba	0.00	0.00	0.01	0.01	0.01
Total	5.02	5.01	5.08	5.07	5.23
An (mol%)	27.70	44.64	7.53	3.93	2.19
Ab (mol%)	69.41	52.12	90.10	91.44	94.50
Or (mol%)	2.89	3.24	2.38	4.63	3.31

The incorporation of Na and Ca into altered rocks is typical for this type of alteration in porphyry-copper deposits, and it is described in numerous publications (e.g., Dilles et al. 1995; Halley et al. 2015). The Na–Ca alteration has a complicated intimate relationship with the K-silicate alteration, related to the superimposition of the Na–Ca alteration or vice-versa in some places. This type of relationship is also noted by other researchers in connection with the pulsative nature of porphyry systems (e.g., Carten 1986; Melfos et al. 2020). The spatial distribution of the alteration (not limited only to veins) suggests participation of a significant volume of fluid phase, while petrographic observations indicate almost simultaneous formation of the Na–Ca and the K-silicate alterations. Nevertheless, at the deposit the earliest fluids contain just a little or no CO_2 (Stefanova et al. 2014), so they cannot form the Na–Ca alteration on their own (e.g., Li et al. 2018). For porphyry-copper deposits related to calc-alkaline magmatic systems (such as Elatsite) some authors suggest its formation from external fluids, as fracturing caused by exceeding the fluid pressure over the lithostatic pressure during the release of magmatic fluids may provide pathways for the circulation of saline-basinal, surface-derived external fluids or recirculated magmatic brines (e.g., Seedorff et al. 2008). For Elatsite we suggest that the heated non-magmatic fluids from the metamorphic basement, rich in carbonate components, are of

Table 5: Representative microanalyses and calculated formulae (on the basis of 28 O) of hydrothermal chlorites from propylitic alteration (Chl 1), Chl 2 from K-silicate–sericitic alteration developed on secondary biotite from K-silicate alteration (Chl 2) and developed on secondary biotite from Na–Ca–K-silicate alteration (Chl 2-1). chlorite from quartz–adularia–carbonate alterations (Chl 3). The main oxides in wt%. FeO* total iron as FeO; Fe*=Fe/Fe+Mg.

	Chl 1						Chl 2			Chl 2-1			Chl 3		
	Hb	Hb	Px	Px	Bt	Bt							vein	vein	vein
SiO_2	28.71	26.56	30.90	31.02	28.68	28.88	26.83	28.05	27.46	28.14	29.67	28.01	27.00	31.32	30.97
TiO2	0.00	0.00	0.00	0.00	0.00	0.00	0.00	2.02	0.13	0.00	0.00	0.41	0.20	0.00	0.13
Al_2O_3	21.00	19.30	17.56	17.27	20.85	20.40	21.41	17.75	19.80	15.80	16.54	14.13	21.07	22.28	22.73
FeO*	21.24	23.33	14.01	13.48	21.65	20.33	17.60	16.19	14.96	29.55	24.34	29.86	15.77	9.94	7.79
MnO	0.41	0.77	0.46	0.36	0.41	1.37	0.38	0.68	0.28	0.14	0.10	0.10	0.40	0.14	0.30
MgO	18.06	14.25	24.47	25.01	18.31	17.62	19.64	19.31	20.84	14.93	17.00	15.28	20.70	24.53	24.22
CaO	0.11	0.60	0.49	0.37	0.06	0.17	0.45	1.02	0.56	0.34	0.10	0.08	0.44	0.30	0.50
K_2O	0.14	1.33	0.31	0.31	0.08	0.11	0.36	0.75	0.29	0.03	0.20	0.13	0.35	0.23	0.33
Cl	0.07	0.29	0.32	0.32	0.05	0.08	0.33	0.29	0.32	0.03	0.04	0.03	0.35	0.16	0.28
Total	89.74	86.43	88.52	88.14	90.09	88.96	87.00	86.06	84.64	88.96	87.99	88.03	86.28	88.90	87.25
Si	5.70	5.53	6.02	6.07	5.70	5.78	5.44	5.73	5.64	5.47	5.64	5.77	5.49	5.88	5.85
Al^{iv}	2.30	2.47	1.98	1.93	2.30	2.22	2.56	2.27	2.36	2.53	2.36	2.23	2.51	2.12	2.15
Al^{vi}	2.64	2.36	2.07	2.08	2.61	2.63	2.59	2.04	2.47	1.17	1.41	1.25	2.56	2.86	2.97
Ti	0.00	0.00	0.00	0.00	0.00	0.00	0.00	0.31	0.02	0.00	0.00	0.06	0.03	0.00	0.02
Fe^{3+}	0.19	0.00	0.11	0.12	0.16	0.21	0.07	0.21	0.14	0.00	0.00	0.00	0.10	0.42	0.51
Fe^{2+}	3.34	4.24	2.17	2.09	3.44	3.20	2.92	2.55	2.43	7.16	6.16	6.37	2.58	1.14	0.72
Mn	0.07	0.14	0.08	0.06	0.07	0.23	0.07	0.12	0.05	0.02	0.02	0.02	0.07	0.02	0.05
Mg	5.35	4.43	7.11	7.30	5.43	5.26	5.94	5.88	6.39	4.32	4.82	4.69	6.27	6.87	6.82
Ca	0.02	0.13	0.10	0.08	0.01	0.04	0.10	0.22	0.12	0.07	0.02	0.02	0.10	0.06	0.10
K	0.07	0.71	0.15	0.15	0.04	0.06	0.19	0.39	0.15	0.01	0.10	0.07	0.18	0.11	0.16
Ba	0.00	0.16	0.08	0.00	0.00	0.00	0.13	0.17	0.10	0.00	0.00	0.00	0.04	0.00	0.04
Cl	0.05	0.20	0.21	0.21	0.03	0.05	0.23	0.20	0.22	0.02	0.03	0.02	0.24	0.10	0.18
OH*	15.95	15.80	15.79	15.79	15.97	15.95	15.77	15.80	15.78	15.98	15.97	15.98	15.76	15.90	15.82
Total	35.81	36.76	36.62	36.57	35.83	35.82	36.02	35.89	35.89	36.84	36.69	36.57	35.93	35.49	35.41

key importance for the formation of the Na–Ca alteration. During the emplacement of the porphyritic magmas, temperature increases, and the fluid-rock interaction can mobilize CO_2 from schists of the basement, which probably have caused the spatial manifestation of the Na–Ca alteration. Similar events have been described in other papers (e.g., Dilles & Einaudi 1992).

The geochemical behavior of elements in the Na–Ca–K-silicate alteration shows many similarities with earlier studies of the K–Na alteration in porphyry-copper deposits (e.g., Zhang et al. 2023). We suggest that the transitional features of the Na–Ca–K-silicate alteration are related to its formation in an environment with a high oxygen fugacity (described by the presence of magnetite in the corresponding mineral assemblage) from fluids with a relatively low salinity (Cl^- content in secondary biotites is close to values in igneous biotites). Barium contents in hydrothermal biotite are transitional between the low values in igneous biotites and higher values of hydrothermal biotites in the K-silicate alteration, and estimated temperatures of their crystallization are close to magmatic temperatures (average about 720 °C). The transitional features of the secondary biotites from the Na–Ca–K-silicate alteration probably indicate formation in zones of primary neutralization (Giggenbach 1988; Hedenquist & Lowenstern 1994). Similarities of the chemistry of biotite and amphibole from the Na–Ca–K-silicate alteration with the primary biotite and amphibole, suggest a temperature and chemical equilibrium between the early released fluids and the host rocks (granodiorite porphyrites), while the characteristics of plagioclase probably reflect the changing a_{Ca}/a_{Na} ratio in the fluids, probably as a result of incorporation of an external fluid.

The data obtained for the K-silicate alteration and the K-silicate–sericitic alteration show many similarities with previous studies of alteration in porphyry deposits (e.g., Ford 1978; Anthony & Titley 1994; Ulrich & Heinrich 2002; Idrus et al. 2009; Höss et al. 2024). The high contents of Na_2O in the K-silicate alteration at the deposit are probably the result of an increase of the albite component in the plagioclase composition (Georgiev 2019). Some authors propose that the loss of Ca from the K-silicate alteration is linked to its accumulation in the propylitic alteration (e.g., Ford 1978; Ulrich & Heinrich 2002). However, in the Elatsite deposit, no relationship between these two alterations has been observed, and the timing of their formation remains unclear. The depletion of Ca in the K-silicate alteration may be related to the breakdown of primary amphiboles during their alteration to biotite, as well as the increase of Na at the expense of Ca in plagioclase, with some of the Ca released by both mechanisms and being trapped by anhydrite, when sulfate is present (Camus 1975). The Mg depletion of K-silicate altered rocks is also documented by Georgiev (2019). Other authors also reported a decrease in Mg in similar rocks from porphyry deposits (e.g., Camus 1975; Taylor & Fryer 1980), resulting from the breakdown of mafic minerals. The K-silicate alteration is the first alteration type to occur due to the release of magmatic fluids (e.g., Strashimirov et al. 2002; Georgiev 2008; Stefanova et al. 2014). The explosive release of fluids causes fracturing of the host rock and the first site of occurrence of the K-silicate alteration are cracks conduits, where the alteration is observed in veins. Two pulses of the K-silicate alteration are observed at the deposit (Ivanov et al. 2014) and the superimposition of one pulse over another is typical for the Elatsite rocks (Fig. 13a). Nevertheless, no or negligible differences were observed in the geochemistry of the two pulses. The K-silicate alteration occurs in an environment with a high oxygen fugacity with magnetite and hematite in the assemblage, and at average temperatures 709 °C which are close to magmatic (Georgieva & Nedialkov 2017a) with the mineral assemblage of biotite, potassium feldspar, magnetite, anhydrite, minor hematite, zircon, apatite, and quartz. Secondary biotite from the K-silicate alteration with higher Mg* ratio and lower Ti and Ba values than the magmatic biotite is described in the same alteration type in many other porphyry-copper deposits (e.g., Jacobs & Parry 1979; Hendry et al. 1985; Melfos et al. 2020). The formation of secondary biotite from an environment with a high oxygen fugacity is not unusual for porphyry systems and probably reflects formation from early high-temperature fluids (e.g., Chivas 1981; Melfos et al. 2020). The overall REEs depletion of the rocks affected by the K-silicate alteration (relative to unaltered rocks) probably indicates a high Cl^- activity (Taylor & Fryer 1980) in the earliest fluids, as indicated by the high Cl^- values of hydrothermal biotites from the K-silicate alteration and high salinity of fluid inclusions in quartz associated with the K-silicate alteration (Strashimirov et al. 2002; Tarkian et al. 2003; Stefanova 2009; Stefanova et al. 2014). Probably hot (above 400 °C) and Cl-rich fluids have mobilized REEs, like reported in other porphyry copper systems (e.g., van Dongen et al. 2010; Höss et al. 2024).

Two types of the K-silicate–sericitic alteration are present at the deposit: with the dominance of chlorite or with the dominance of sericite. To initiate the chloritization aH^+ consumption and depletion in a_{K+}/a_{H+} ratio is required (e.g., Beane 1974; Parry & Downey 1982), suggesting an incorporation of meteoric fluids in the formation of the K-silicate–sericitic alteration. The a_{Mg} remains high as the newly formed chlorites have higher Mg* ratio values, and the presence of H^+ in the system is probably related to its incorporation by meteoric fluids. K^+ is incorporated into fluids with the alteration of biotite to chlorite (Parry & Downey 1982) and the a_{K+}/a_{H+} ratio of the solutions increases. A similar H–K metasomatism is present in different models (Giggenbach 1988). Figure 12 illustrates the changing ratio of a_{K+}/a_{H+} and a_{Mg2+}/a_{H+} in fluids. Following the formation of the K-silicate alteration and the decrease in a_{K+} (while a_{Mg2+} remains high), the K-silicate–sericitic alteration develops. In the very initial stage, the alteration is associated with a highly oxidizing environment, which leads to the formation of magnetite and hematite, but passes into pyrite and chalcopyrite formation in the later and more intense stages of alteration. Probably the incorporation of external fluids from the basement to the magmatic fluid increased a_{CO2} and a_{Ca2+} in the solutions and consequently lead to the formation of Ca-rich minerals (as prehnite) in

the K-silicate-sericitic alteration. The admixture of meteoric fluid to magmatic fluid at temperatures below 480 °C and pressures slightly above 0.2 kbar is suggested for the rocks in the Elatsite deposit based on fluid inclusions data from the associated quartz (Fekete et al. 2016), which corresponds to the environment of the K-silicate–sericitic alteration from the present study. The admixture of meteoric fluid into magmatic fluid at the Elatsite deposit is documented by low-temperature, low-salinity fluid (Tarkian et al. 2003).

For the geochemical distribution of elements in the quartz–sericite alteration there exist many similarities with previous studies (e.g., Scott 1978; Ulrich & Heinrich 2002; Hikov 2013; Li et al. 2013; Höss et al. 2024). The comparison of our data with the data obtained by Georgiev (2019) reveals some differences for the quartz–sericite alteration, like lower contents of K_2O and an ambiguous behavior of Na_2O. The geochemical data of the quartz–sericite alteration suggests an enrichment in K^+ in the rocks compared to the K-silicate–sericitic alteration. The K^+ released with the chloritization of secondary biotite participate in the formation of white micas from the quartz–sericite alteration (Ford 1978). Sericite from the alteration is also characterized by a higher Cl^- content, which is probably related to the higher salinity of the solutions (Georgieva et al. 2024b). The higher a_{H+} shown in Fig. 12 suggests an acidic environment of the fluids, which favors the release of REEs and metals and their incorporation into the fluid phase. This corresponds to the decreasing REEs content in the rocks. The temperature of formation of the quartz–sericitic alteration is estimated about 260–300 °C and it could be the result of entirely magmatic fluids with a decreasing K^+/H^+ ratio or the result of meteoric hydrothermal fluids (Georgiev 2019).

The data obtained for the propylitic alteration shows correlation with data for the same alteration in other porphyry systems (e.g., Ulrich & Heinrich 2002; Idrus et al. 2009; Hikov 2013). The exchange of Ca^{+2} by K^+ and Na^+ is essential for the propylitic alteration, which is accompanied by significant desilification (Ulrich & Heinrich 2002). The slight reduction of Ca^{+2} in the propylitic alteration may be attributed to its presence in primary minerals like plagioclase and amphibole, and its subsequent release during fluid-rock interactions, rather than its preservation in epidote and calcite (e.g., Garwin 2002; Idrus et al. 2009). The propylitic alteration is the least studied alteration at the deposit, as it occurs mainly outside of the open pit, with temperatures of formation at about 175–318 °C (Georgieva & Nedialkov 2017b). The simultaneous formation of the propylitic and the K-silicate alterations in the deposit was described by Georgiev (2019), but our data does not confirm this interpretation.

The quartz–adularia–carbonate alteration is one of the latest alteration types at the deposit. This low-temperature K-metasomatism (Georgiev 2019) has a clear structural control, being observed as veins and nests in the matrix of porphyries and granodiorites of the pluton. The presence of the carbonate–zeolite paragenesis (roughly coinciding with the quartz–adularia–carbonate alteration) is described in large areas, and

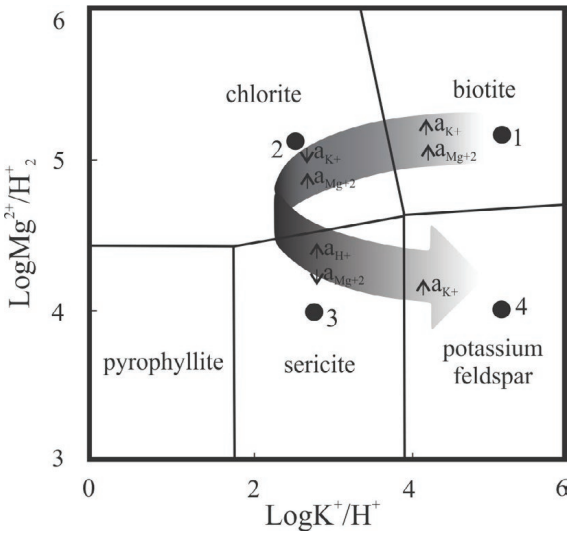

Fig. 12. Diagram log Mg^{+2}/H^{+2} vs. log K^+/H^+ showing mineral equilibrium in the system H_2O-gas. Grey arrow shows the evolution trend of fluids and numbers the location of the K-silicate alteration (1), K-silicate–sericitic alteration (2), quartz–sericitic alteration (3) and quartz–adularia–carbonate alteration (4). Smaller arrows show high (↑) and low (↓) activity of respective elements (after Beane & Bodnar 1995).

according to Kehayov (2005), the distribution of this type of mineralization is related to the reactivation of cracks during the last fragile tectonic disturbances in the deposit. The temperature estimations for the formation of chlorite in this alteration type are about 248–304 °C, which are higher than the temperature of homogenization of fluid inclusions in quartz associated with the post-sulfide zeolite–carbonate assemblage (Stefanova et al. 2014). The occurrence of adularia requires a high a_{K+} and a high a_{K+}/a_{H+} ratio (Fig. 12), while the formation of albite, which is also locally present in this alteration, requires a high a_{Na+} and a high a_{Na+}/a_{H+} ratio. The elevated contents of K^+ in the fluids is probably related to the evolving magmatic fluid, while a part of K^+ was probably incorporated into the fluids during the fluid–rock interaction. The formation of the quartz–adularia–carbonate alteration is probably related to the evolution of the magmatic-hydrothermal fluids (as a source of sulfur and K^+), as well as to the incorporation of meteoric and other external fluids, rich in CO_2 and Ca^{+2}, for the formation of carbonate minerals, epidote, and prehnite. The variable mineral composition of this alteration is probably the result of the changing ratio between the three components in the system and variations in temperature.

Model of the magmatic-hydrothermal system

The model of the magmatic-hydrothermal system associated with the Elatsite porphyry copper deposit is heavily influenced by the pulsative nature of the magmatic activity and the emplacement of several Upper Cretaceous porphyries, primarily quartz-monzodiorite and granodiorite porphyries.

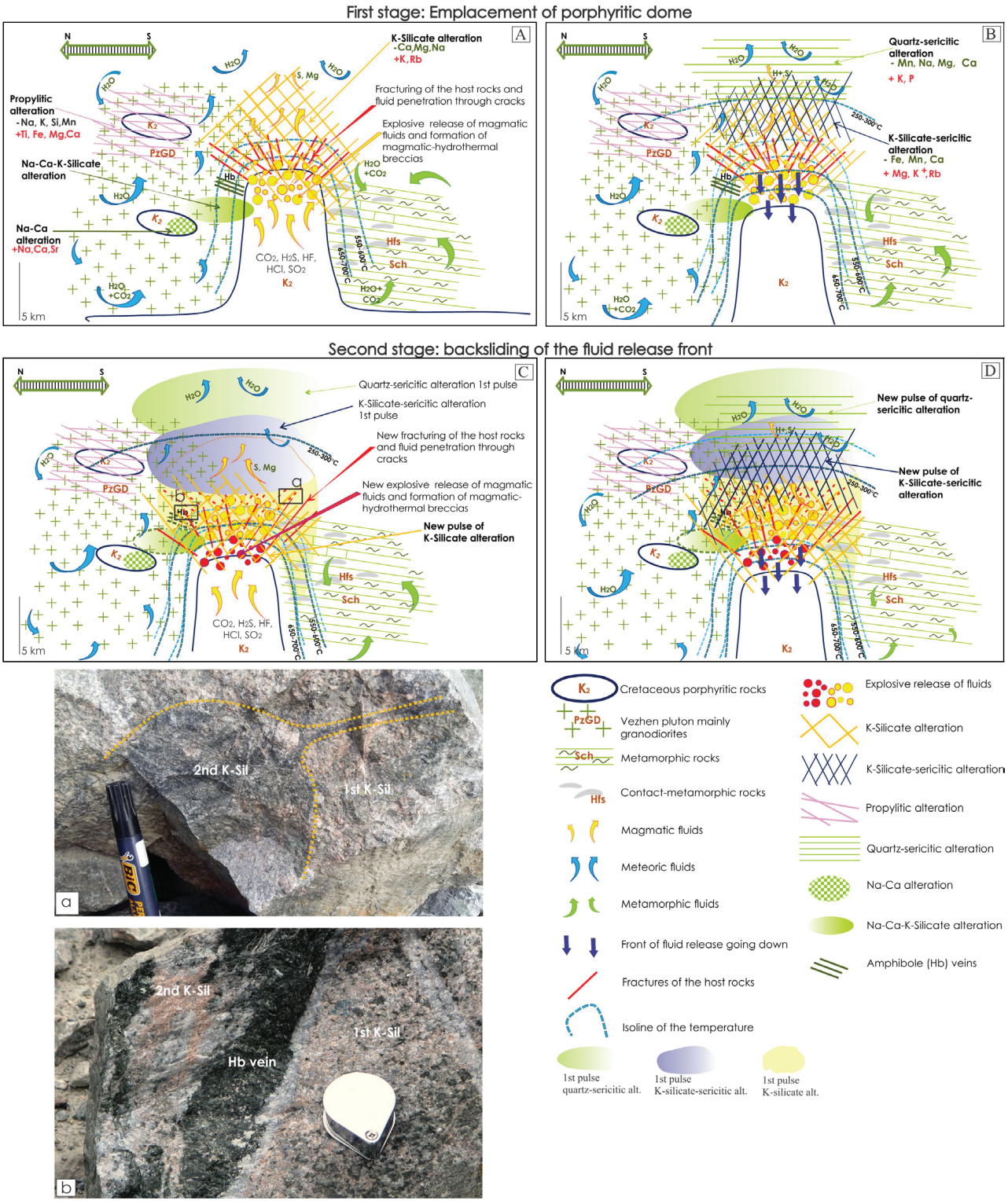

Fig. 13. Model of evolution of the magmatic-hydrothermal system in the Elatsite deposit in two stages. **(A)** and **(B)** show the first evolutionary stage, related to the emplacement of the porphyritic dome; **(C)** and **(D)** show the second stage, related to the backsliding of the front of fluids release. **(a)** Second pulse of K-silicate alteration intruded into previously formed K-silicate alteration; **(b)** Second pulse of the K-silicate alteration imposed over Na–Ca alteration (Hb veins) in granodiorite of the Vezhen pluton also affected by the first pulse of the K-silicate alteration (after Georgieva et al. 2019).

The hydrothermal system begins with the emplacement of quartz-monozdiorite porphyry, when an explosive release of fluids and the formation of magmatic-hydrothermal breccias happened (Fig. 13A). The rock fracturing provided pathways for the earliest fluids and the K-silicate alteration occurred initially around cracks. As the intensity of alteration increased, it affected both the Upper Cretaceous dyke and the Vezhen pluton. The fluids involved are characterized by the incorporation of K^+, a high a_{K+}/a_{H+} ratio, high salinity, high oxidation potential, and high temperature. At the periphery of the dome, magmatic fluids with high temperature were active, and the cracks in the host rocks served as pathways for the formation of amphibole veins. During this time, the magmatic chamber heated the basement, leading to continuous circulation of external fluids, while mixing of magmatic fluids with external fluids probably resulted in the Na–Ca alteration in the peripheral zones. The external fluids probably prevailed and were likely of a lower temperature than those involved in the Na–Ca–K-silicate alteration. The K-silicate alteration, the Na–Ca–K-silicate alteration and the Na–Ca alteration occurred almost simultaneously, with complex and ambiguous relationships determined by the pulsative nature of the Upper Cretaceous magmatic activity. In the periphery of the dome in the country rocks the propylitic alteration was formed by the predominance of meteoric fluids. From the available data, it is not possible to determine the time of formation of this alteration and its relationship with other alterations, but it is characterized by formation temperatures of about 240–340 °C and a relatively low a_{K+}/a_{H+} ratio.

The fluid–fluid interaction of magmatic and meteoric fluids in upper parts of the dome resulted in the formation of the K-silicate–sericitic alteration, which overprints the K-silicate and Na–Ca–K-silicate alterations, when the boundary between the meteoric and magmatic fluid flow moved downward (Fekete et al. 2016, Fig. 13B). The spatial distribution of this alteration was strongly related to the presence of the K-silicate alteration and partially of the Na–Ca–K-silicate alteration. The characteristics of the newly formed minerals inherited the characteristics of earlier primary or secondary minerals (Georgieva & Nedialkov 2021). As the alteration of secondary biotite to chlorite or sericite released H^+, it acidified the environment and reduces the a_{K+}/a_{H+} ratio (Fig. 12). The oxidation potential of the fluids decreased after the formation of the K-silicate–sericitic alteration. The released H^+ and incorporation of meteoric fluid by fluid-fluid interactions resulted in the quartz–sericitic alteration, formed predominantly by meteoric fluid with a low a_{K+}/a_{H+} ratio, while S and partially Fe were probably provided by magmatic fluids. One of the last alteration types observed at the deposit is the quartz–adularia–carbonate alteration, which is superimposed on all previously formed alteration types. It is not presented in the model due to its limited spatial distribution and clear structural control. The argillic-like alteration is also not represented in the model due to the limited data for this type of alteration.

During the second stage, a new pulse of porphyritic magmas arose, accompanied by the release of magmatic fluids. This, however, occurred at a lower part of the system, due to the backsliding of the fluid release front, as suggested by Burnham (1985). Exceeding the fluid pressure above the lithostatic pressure led to a new explosive release of fluids and a new formation of magmatic-hydrothermal breccias, which was associated with a new manifestation of the K-silicate alteration (Fig. 13C). This new alteration pulse was superimposed on the already formed K-silicate alteration and the Na–Ca alteration from the previous pulse, as shown in Fig. 13a. The characteristics of the alteration and the mineral composition do not differ significantly from the previous ones. The new pulse affected all the previously formed alterations and included amphibole veins and the K-silicate alteration (Fig. 13b). This mechanism explains the imposition of higher temperature on lower temperature alterations which is typical for the deposit. The evolution of the fluids associated with this new pulse does not differ from the evolution of the previous one. The penetration of meteoric fluids continued, as well as the upward movement of magmatic fluids (Fig. 13D).

The pulsative nature of magmatism, multiple sources of hydrothermal fluids and their evolution are the reason for the formation of variety of hydrothermal alteration types and their diverse mineral compositions. The united model of the deposit improves the understanding of the evolution of the magmatic-hydrothermal system in the porphyry-copper deposits.

Acknowledgments: The study was supported by the KP-06-N44/4 project, financed by the Bulgarian National Science Fund. We highly appreciate the notes and comments from the reviewers and the editorial board for improving the manuscript.

References

Afshooni S.Z., Mirnejad H., Esmaeily D. & Haroni H.A. 2013: Mineral chemistry of hydrothermal biotite from the Kahang porphyry Copper Deposits (NE Isfahan), Central Province of Iran. *Ore Geology Reviews* 54, 214–232. https://doi.org/10.1016/j.oregeorev.2013.04.004

Anthony E. & Titley S. 1994: Patterns of element mobility during hydrothermal alteration of the Sierrita porphyry copper deposit, Arizona. *Economic Geology* 89, 186–192. https://doi.org/10.2113/gsecongeo.89.1.186

Antonov M. & Jelev V. 2002: Ductile shear zone and brittle faults in the Southwestern slope of Zlatitsa-Teteven Mountain (Central Bulgaria). *Annual of the University of Mining and Geology "St. Ivan Rilski"* 45, I, 13–20.

Augé T., Bailly L. & Petronov R. 2005: On the origin of the PGE mineralization in the Elatsite Porphyry Cu-Au Deposit: Comparison with the Baula-Nuasahi Complex, India and other alkaline PGE-rich porphyries. *Canadian Mineralogist* 43, 1355–1372. https://doi.org/10.2113/gscanmin.43.4.1355

Beane R.E. 1974: Biotite stability in the porphyry copper environment. *Economic Geology* 69, 241–256. https://doi.org/10.2113/gsecongeo.69.2.241

Beane R.E. & Bodnar R.J. 1995: Hydrothermal fluids and hydrothermal alteration in porphyry copper deposits. In: Pierce F.W. & Bohm J.G. (Eds.): Porphyry copper deposits of the American Cordillera. *Arizona Geological Society Digest* 20, 83–93.

Bogdanov B. 1987: Copper deposits in Bulgaria. *Tehnika*, Sofia, 1–388 (in Bulgarian).

Bogdanov K., Filipov A. & Kehayov R. 2005: Au–Ag–Te–Se minerals in the Elatsite porphyry-copper deposit, Bulgaria. *Geochemistry, Mineralogy and Petrology* 43, 13–19.

Boynton W. 1984: Cosmochemistry of the rare earth elements: Meteorite study. In: Henderson R. (Eds.): Rare Earth Elements Geochemistry. *Elsevier*, Amsterdam, 63–114. https://doi.org/10.1016/B978-0-444-42148-7.50008-3

Burnham C.W. 1979: Magma and hydrothermal fluids. In: Barnes H.L. (Ed.): Geochemistry of hydrothermal ore deposits. *2nd ed., Wiley Interscience*, New York, 71–136.

Burnham C.W. 1985: Energy release in subvolcanic environments: Implication for breccia formation. *Economic Geology* 80, 1515–1522. https://doi.org/10.2113/gsecongeo.80.6.1515

Byrne K., Lesage G., Gleeson S.A., Piercey S.J., Lypaczewski P. & Kyser K. 2020: Linking Mineralogy to Lithogeochemistry in the Highland Valley Copper District: Implications for Porphyry Copper Footprints. *Economic Geology* 115, 871–901. https://doi.org/10.5382/econgeo.4733

Camus F. 1975: Geology of the El Teniente orebody with emphasis on wall-rock alteration. *Economic Geology* 8, 1341–1372. https://doi.org/10.2113/gsecongeo.70.8.1341

Carten R.B. 1986: Sodium-calcium metasomatism; chemical, temporal, and spatial relationships at the Yerington, Nevada, porphyry copper deposit. *Economic Geology* 81, 1495–1519. https://doi.org/10.2113/gsecongeo.81.6.1495

Chivas A.R. 1981: Geochemical evidence for magmatic fluids in porphyry copper mineralization. *Contribution to Mineralogy and Petrology* 78, 389–403. https://doi.org/10.1007/BF00375201

Ciobanu C., Cook N.G. & Stain H. 2002: Regional setting and geochronology of the Late Cretaceous Banatitic magmatic and metallogenic belt. *Mineralium Deposita* 37, 541–567. https://doi.org/10.1007/s00126-002-0272-9

Davies J.F. & Whitehead R.E. 2010: Alkali/alumina molar ratio trends in altered granitoid rocks hosting porphyry and related deposits. *Exploration and Mining Geology* 19, 13–22. https://doi.org/10.2113/gsemg.19.1-2.13

Deer W.A., Howie R.A. & Zussman J. 1992: An Introduction to rock forming minerals. *Longman*, 1–696.

Dilles J.H. & Einaudi M.T. 1992: Wall-rock alteration and hydrothermal flow paths about the Ann-Mason porphyry copper deposit, Nevada – a 6-km vertical reconstruction. *Economic Geology* 87, 1963–2001. https://doi.org/10.2113/gsecongeo.87.8.1963

Dilles J.H., Solomon G.C., Taylor H.P. & Einaudi M.T. 1992: Oxygen and hydrogen isotope characteristics of hydrothermal alteration at the Ann-Mason porphyry copper deposit, Yerington, Nevada. *Economic Geology* 87, 44–63. https://doi.org/10.2113/gsecongeo.87.1.44

Dilles J.H., Farmer G.L. & Field C.W. 1995: Sodium-calcium alteration by non-magmatic saline fluids in porphyry copper deposits: Results from Yerington, Nevada. In: Thompson J.F.H. (Eds): Magmas, Fluids, and Ore Deposits. *Mineralogical Association of Canada, Short Course Series* 23, 309–338.

Dragov P. & Petrunov R. 1996: Elatsite porphyry-copper – precious metals (Au and PGE) deposit. In: Popov P. (Ed.): Plate tectonic aspects of the Alpine metallogeny in the Carpatho-Balkan region. *Proceedings of Annual meeting, Sofia* 1, 171–175.

Fekete Sz., Weis Ph., Driesner Th., Bouvier A-S., Baumgartner L. & Heinrich C. 2016: Contrasting hydrological processes of meteoric water incursion during magmatic–hydrothermal ore deposition: An oxygen isotope study by ion microprobe. *Earth and Planetary Science Letters* 451, 263–271. https://doi.org/10.1016/j.epsl.2016.07.009

Ford J.H. 1978: A chemical study of alteration at the Panguna porphyry copper deposit, Bougainville, Papua New Guinea. *Economic Geology* 73, 703–720. https://doi.org/10.2113/gsecongeo.73.5.703

Garwin S. 2002: The geologic setting of intrusion-related hydrothermal systems near the Batu Hijau porphyry copper-gold deposit, Sumbawa, Indonesia. In: Goldfarb R.J. & Nielsen R.L. (Eds.): Integrated methods for discovery: global exploration in the twenty-first century. *Society of Economic Geologists*, Denver, Colorado, 333–366. https://doi.org/10.5382/SP.09.15

Georgiev G. 2004: Geology of porphyry-copper deposit Elatsite, Bulgaria. *Annual of the University of Mining and Geology "St. Ivan Rilski", Geology and Geophysics* 47, 75–82.

Georgiev G. 2008: A genetic model of the Elatsite porphyry copper deposit, Bulgaria. *Geochemistry, Mineralogy and Petrology* 46, 143–160.

Georgiev G. 2019: Hydrothermal metasomatites in Elatsite porphyry copper deposit. *Scientific and Technical Union of Mining, Geology and Metallurgy*, Sofia, 57–99.

Georgiev N., Krumov I., Nanov Z., Elenkov K., Naydenov K., Milenkov G., Karakolev Al. & Markov G. 2020: Tabular preparation and three-dimensional modeling of drilling data related to the spatial distribution of hydrothermal alterations in the Elatsite deposit in M 1:2000 in 2020. *Archive of Elatsite-Med AD*.

Georgiev N., Nanov Z., Elenkov K., Naydenov K., Milenkov G., Karakolev Al. & Markov G. 2023: Geological-structural and engineering-geological (geotechnical) mapping of newly discovered mine slopes in M 1:500 in 2023. *Archive of Elatsite-Med AD*.

Georgiev S., Gerdjikov I., Peytcheva I. & Makaveev P. 2020: Time frame of the Carboniferous tectonic and magmatic activity in the area of Vezhen pluton, Bulgaria. *Review of the Bulgarian Geological Society* 81, 72–74.

Georgieva H & Nedialkov R. 2017a: Geochemical characteristics of igneous and hydrothermal biotites from Elatsite porphyry-copper deposit, Bulgaria. In: *Proceedings of the National conference "Geosciences"*, 51–52.

Georgieva H & Nedialkov R. 2017b: Chlorite from Elatsite PCD, as a mineral vector. *Proceeding in Goldschmidt Abstracts*, 1319.

Georgieva H. & Nedialkov R. 2021: Chemistry of chlorite from the K-silicate-sericitic alteration in Elatsite porphyry Cu-Au deposit, Bulgaria. *Review of the Bulgarian Geological Society* 82, 52–54. https://doi.org/10.52215/rev.bgs.2021.82.3.52

Georgieva H., Nedialkov R. & Krumov I. 2019: Hydrothermal amphiboles from Na–Ca and Na–Ca–K–Silicate alterations: An example from Elatsite porphyry copper-gold deposit, Bulgaria. In: *Proceedings of the Geologica Carpathica 70*, 65–68.

Georgieva H., Nedialkov R., Stefanova E., Milenkov G., Krumov I. & Georgiev N. 2023: Preliminary data on the mineral chemistry of garnet from the skarn alteration associated with the Elatsite porphyry-copper deposit, Bulgaria. *Review of the Bulgarian Geological Society* 84, 31–34. https://doi.org/10.52215/rev.bgs.2023.84.3.31.

Georgieva H., Nedialkov R., Stefanova E. & Milenkov G. 2024a: Mineral chemistry of hydrothermal biotite from Na–Ca–K-silicate alteration associated with the Elatsite porphyry copper deposit, Bulgaria. In: *Proceeding in European Mineralogical Conference*, Dublin, 258.

Georgieva H., Nedialkov R., Stefanova E. & Milenkov G. 2024b: Chemical composition of white micas from the Elatsite porphyry copper deposit, Bulgaria. *Review of the Bulgarian Geological Society* 85, 163–166. https://doi.org/10.52215/rev.bgs.2024.85.2.163.

Gerdjikov I. & Georgiev N. 2006: The Svishti Plaz Allochthon (Central Balkanides). Position and associated fabric. *Comptes rendus de l'Académie bulgare des Sciences* 59, 631–638.

Gerdjikov I., Kounov A., Lazarova A., Georgiev S. & Vangelov D. 2023: Lower Paleozoic low-grade metamorphic units from the Central Balkan Zone, Bulgaria: tectonic relationships, framework and geodynamic significance. *Geologica Balcanica* 52, 65–86. https://doi.org/10.52321/GeolBalc.52.1.65

Giggenbach W. 1988: Geothermal solute equilibria. Derivation of Na–K–Mg–Ca geoindicators. *Geochimica et Cosmochimica Acta* 52, 2749–2765. https://doi.org/10.1016/0016-7037(88)90143-3

González-Jiménez J.M., Piña R., Kerestedjian T., Gervilla F., Borrajo I., Farré-de Pablo J., Proenza J.A., Tornos F., Roqué J. & Nieto F. 2021: Mechanisms for Pd–Au enrichment in porphyry-epithermal ores of the Elatsite deposit, Bulgaria. *Journal of Geochemical Exploration*, 220. https://doi.org/10.1016/j.gexplo.2020.106664

Hadzhieva N. 2009: Geology and petrography of magmatic and magmatic-hydrothermal breccias from explosive pipes in Elatsite deposit. *Master Thesis*, *Sofia University*, Sofia, 1–117 (in Bulgarian).

Halley S., Dilles J. & Tosdal R. 2015: Footprints: The hydrothermal alteration and geochemical dispersion around porphyry copper deposits. *SEG Newsletter*, no. 100.

Handler R., Neubauer F., Velichkova S. & Ivanov Z. 2004: $^{40}Ar/^{39}Ar$ age constraints on the timing of magmatism in the Panagyurishte region, Bulgaria. *Schweizerische Mineralogische und Petrographische Mitteilungen* 84, 133–151.

Hawthorne F.C., Oberti R., Harlow G.E., Maresch W.V., Martin R.F., Schumacher J.C. & Welch M.D. 2012: Nomenclature of the amphibole supergroup. *American Mineralogist* 97, 2031–2048. https://doi.org/10.2138/am.2012.4276

Hedenquist J.W. & Lowenstern J.B. 1994: The role of magmas in the formation of hydrothermal ore deposits. *Nature* 370, 519–527.

Heinrich C. & Neubauer F. 2002: Cu–Au–Pb–Zn–Ag metallogeny of the Alpine–Balkan–Carpathian–Dinaride geodynamic province. *Mineralium Deposita* 37, 533–540. https://doi.org/10.1007/s00126-002-0271-x

Hendry D.A.F., Chivas A.R., Long J.V.P. & Reed S.J.B. 1985: Chemical differences between minerals from mineralizing and barren intrusions from some North American porphyry copper deposits. *Contributions to Mineralogy and Petrology* 89, 317–329. https://doi.org/10.1007/BF00381554

Henry D.J., Guidotti C.V. & Thomson J.A. 2005: The Ti-saturation surface for low-to-medium pressure metapelitic biotites: Implications for geothermometry and Ti-substitution mechanisms. *American Mineralogist* 90, 316–328. https://doi.org/10.2138/am.2005.1498

Hikov A. 2013: Geochemistry of hydrothermally altered rocks from the Asarel porphyry copper deposit, Central Srednogorie. *Geologica Balcanica* 42, 3–28. https://doi.org/10.52321/GeolBalc.42.1-3.3

Hollister V. 1978: Geology of porphyry copper deposits of the western hemisphere. *Society of Mining Engineers of the American Institute of Mining, Metallurgical, and Petroleum Engineers*, 1–219.

Höss A., Haase K.M., Keith M., Klemd R., Melfos V., Gerlach L., Pelloth F., Falkenberg J.J., Voudouris P., Strauss H., Baker T. & Tarantola A. 2024: Magmatic and hydrothermal evolution of the Skouries Au–Cu porphyry deposit, northern Greece. *Ore Geology Reviews* 173. https://doi.org/10.1016/j.oregeorev.2024.106233

Idrus A., Kolb J. & Meyer F.M. 2009: Mineralogy, lithogeochemistry and elemental mass balance of the hydrothermal alteration associated with the gold-rich Batu Hijau porphyry copper deposit, Sumbawa Island, Indonesia. *Resource Geology* 59, 215–230. https://doi.org/10.1111/j.1751-3928.2009.00092.x

Ivanov Z, Nedialkov R. & Bogdanov K. 2014: Magmatic and ore-related breccias in the Elatsite porphyry-copper deposit (PCD), Bulgaria. *Proceedings of XX CBGA Congress*, Special issue, 158–161.

Jacobs D.C. & Parry W.T. 1979: Geochemistry of biotite in the Santa Rita porphyry copper deposit, New Mexico. *Economic Geology* 74, 860–887. https://doi.org/10.2113/gsecongeo.74.4.860

Janković S., Serafimovski T., Jelenković R. & Cifliganec V. 1997: Metallogeny of the Vardar zone and Serbo-Macedonian mass. In: Boev B. & Serafimovski T. (Eds.): Magmatism, metamorphism, and metallogeny of the Vardar zone and Serbo-Macedonian massif. *Faculty of Mining and Geology*, Štip, 29–38.

Kalaidzhiev S., Hadziiski G. & Angelkov K. 1984: Structural conditions for localization of porphyry copper deposit Elatsite. *Review of the Bulgarian Geological Society* 45, 189–196 (in Bulgarian with English abstract).

Kamenov B., von Quadt A. & Peytcheva I. 2002: New insight into petrology, geochemistry and dating of the Vejen pluton, Bulgaria. *Geochemistry, Mineralogy and Petrology* 39, 3–25.

Kanazirski M. 2011: Hydrothermal wallrock alterations (Physicochemical accents). *Prof. Marin Drinov academic publishing house*, 197–254 (Short version).

Kanazirski M, Chipchakova S., Gorova M. & Arnaudova R. 2002: Wallrock alterations in the porphyry copper deposits of the Panagyurishte ore district and formation–facial belonging of the metasomatites. *Geologica Balkanica* 32, 77–80. https://doi.org/10.52321/GeolBalc.32.2-4.77

Kehayov R. 2005: Mineral assemblages of gold and conditions of their formations in the Elatsite porphyry copper deposit. *PhD Thesis*, *Sofia University*, Sofia, 1–208 (in Bulgarian).

Kehayov R., Bogdanov K., Fanger L., von Quadt A., Pettke T. & Heinrich C. 2003: The fluid chemical evolution of the Elatsite porphyry Cu–Au–PGE deposit, Bulgaria. In: *Proceedings of Society for Geology Applied to Mineral Deposits, SGA Biennial Meeting, 7th Athen, Greece*, 1173–1176.

Kranidiotis P. & MacLean W.H. 1987: Systematics of chlorite alteration at the Phelps Dodge massive sulfide deposit, Matagami, Quebec. *Economic Geology* 82, 1898–1911. https://doi.org/10.2113/gsecongeo.82.7.1898

Lang J.R., Stanley C.R., Thompson J.F.H. & Dunne K.P.E. 1995: Na–K–Ca magmatic-hydrothermal alteration in alkalic porphyry Cu–Au deposits, British Columbia. *Mineralogical Association of Canada, Short Course* 23, 339–366.

Lazarova A. 2008: Shallow-crustal post-tectonic emplacement of Vezhen pluton, Central Stara Planina Mountains. *Comptes rendus de l'Acaddmie bulgare des Sciences* 61, 1315–1322.

Lazarova A., Gerdjikov I., Georgiev N. & Dimov D. 2006: The Anton shear zone (Central Stara Planina Mountains). Temporal relations, extent and significance. *Comptes rendus de l'Académie bulgare des Sciences* 59, 6, 639–644.

Li J., Chen H., Su L., Xiao B. & Wang Y. 2018: Experimental study of high to intermediate temperature alteration in porphyry copper systems and geological implications. *Science China Earth Sciences* 61, 1–21. https://doi.org/10.1007/s11430-018-9295-1

Li X.-C., Fan H.-R., Santosh M., Hu F.-F., Yang K.-F. & Lan T.-G. 2013: Hydrothermal alteration associated with Mesozoic granite-hosted gold mineralization at the Sanshandao deposit, Jiaodong Gold Province, China. *Ore Geology Reviews* 53, 403–421. https://doi.org/10.1016/j.oregeorev.2013.01.020

Lilov P. & Chipchakova S. 1999: K–Ar dating of the Late Cretaceous magmatic rocks and hydrothermal metasomatic rocks from Central Srednogorie. *Geochemistry, Mineralogy and Petrology* 36, 77–91 (in Bulgarian).

Lips A., Herington R., Stein H., Kozelj D., Popov K. & Wijbrans J. 2004: Refined timing of porphyry copper formation in the Serbian and Bulgarian portions of the Cretaceous Carpatho-Balkan Belt. *Economic Geology* 99, 601–609. https://doi.org/10.2113/gsecongeo.99.3.601

Lowell J.D. & Guilbert J.M. 1970: Lateral and vertical alteration-mineralization zoning in porphyry ore deposits. *Economic Geology* 65, 373–408. https://doi.org/10.2113/gsecongeo.65.4.373

MacLean W.H. & Kranidiotis P. 1987: Immobile elements as monitors of mass transfer in hydrothermal alteration: Phelps Dodge Massive sulfide deposit, Matagami, Quebec. *Economic Geology* 82, 951–962. https://doi.org/10.2113/gsecongeo.82.4.951

Madeisky H.E. & Stanley C.R. 1993: Lithogeochemical exploration of metasomatic zones associated with volcanic-hosted massive sulfide deposits using Pearce element ratio analysis. *International Geology Review* 35, 1121–1148. https://doi.org/10.1080/00206819309465580

Melfos V., Voudouris P., Melfou M., Sanchez M.G., Papadopoulou L., Filippidis A., Spry P.G., Schaarschmidt A., Klemd R., Haase K.M., Tarantola A. & Mavrogonatos C. 2020: Mineralogical constrains on the potassic and sodic-calcic hydrothermal alteration and vein-type mineralization of the Maronia porphyry Cu–Mo ± Re ± Au deposit in NE Greece. *Minerals* 10, 182. https://doi.org/10.3390/min10020182

Mladenova V., Apostolova R. & Ivanov Z. 2017: Epithermal intermediate-sulfidation veins in the low-grade metamorphic rocks in the upper levels of the Elatsite porphyry copper deposit, Bulgaria. *Review of the Bulgarian Geological society* 78, 41–54.

Nedialkov R., Hadzhieva N. & Vassileva P. 2012: Geology and petrography of magmatic and magmatic-hydrothermal breccias in porphyry-copper deposit Elatsite. In: *Proceedings of Geological Schools of Bulgaria, the school of prof. Zhivko Ivanov*, 53–56.

Norton D. 1978: Sourcelines, sourceregions, and pathlines for fluids in hydrothermal systems related to cooling plutons. *Economic Geology* 73, 21–28. https://doi.org/10.2113/gsecongeo.73.1.21

Panigrahi M., Kumar Naik R., Pandit D. & Misra K. 2008: Reconstructing physico-chemical parameters of hydrothermal mineralization of copper at the Malanjkhand deposit, India, from mineral chemistry of biotite, chlorite and epidote. *Geochemical Journal* 42, 443–460.

Parry W.T. & Downey L.M. 1982: Geochemistry of hydrothermal chlorite replacing igneous biotite. *Clays and Clay Minerals* 30, 81–90. https://doi.org/10.1346/CCMN.1982.0300201

Petrunov R., Dragov P., Ignatov G., Neykov H., Iliev Ts., Vasileva N., Tsatsov V., Djunakov S. & Doncheva K. 1992: Hydrothermal PGE-minaralization in the Elatsite porphyry copper deposit (the Sredna Gora metallogenic zone, Bulgaria). *Comptes rendus de l'Académie bulgare des Sciences* 45, 37–40.

Peytcheva I., von Quadt A., Georgiev S. & Stoykov S. 2015: Improved U/Pb dating of CA-treated zircons from northern parts of Central Srednogorie for accurate geological interpretation. In: *Proceedings of the National conference "Geosciences"*, 73–74.

Peytcheva I., Loretz M., Von Quadt A., Georgiev S., Kounov A., Gerdjikov I. & Guillong M. 2017a: Time scales of ore deposits: Constraints from U-Pb zircon dating, thermochronology and Sr isotope geochemistry of the porphyry-Cu (Mo–Au) system in Elatsite, Bulgaria. In: *Proceedings of XXXIV International Conference*, 175–179.

Peytcheva I., von Quadt A., Heinrich C., Loretz M., Georgiev S., Kounov A., Gerdjikov I. & Guillong M. 2017b: Timing and scales of magmatic-hydrothermal processes: what we learned from the studies of porphyry-Cu–(Mo–Au) systems. In: *Proceedings of the National conference "Geosciences"*, 63–64.

Popov P. & Popov K. 2022: Metallogeny of Bulgaria. *"BMGK Komers" EOOD publisher*, Sofia, 1–426 (in Bulgarian with extended resume on English).

Popov P., Petrunov R., Kovachev V., Strashimirov S. & Kanazirski M. 2000: Elatsite-Chelopech Ore field. In: Strashimirov S. & Popov P. (Eds.): Geology and metallogeny features of the Panagyurishte ore region (Srednogorie zone, Bulgaria). *ABCD-Geode 2000, Workshop, Borovets, Bulgaria*, 8–18.

Popov P., Berza T., Grubic A. & Dimitru I. 2002: Late Cretaceous Apuseni–Banat–Timok–Srednogorie (ABTS) magmatic and metallogenic belt in the Carpathian–Balkan Orogen. *Geologica Balcanica* 32, 145–163. https://doi.org/10.52321/GeolBalc.32.2-4.145

Popov P., Strashimirov S., Popov K., Kanazirski M., Bogdanov K., Raditchev R., Dimovski S. & Stoykov S. 2012: Geology and metallogeny of the Panagyurishte ore region. *MGU "St. Ivan Rilski" publisher*, Sofia, 1–227 (in Bulgarian with extended English resume).

Roman Alday M.C. 2019: Hydrothermal alteration in Elatsite porphyry Cu–Au–PGE deposit, Bulgaria: A quantitative mineralogy and mineral geochemistry study. *Ms Thesis*, *Université De Gèneve*, 1–176.

Roman Alday M.C., Kouzmanov K., Stefanova E. & Petrov P. 2018: Hydrothermal alteration in the Elatsite porphyry Cu–Au–PGE deposit, Bulgaria: A quantitative mineralogy and mineral geochemistry study. In: *Proceedings of the 16th Swiss Geoscience Meeting, Mineralogy, Petrology, Geochemistry* 2, 2.17.

Scott K.M. 1978: Geochemical aspects of the alteration-mineralization at Copper Hill, New South Wales, Australia. *Economic Geology* 73, 966–976. https://doi.org/10.2113/gsecongeo.73.5.966

Seedorff E., Dilles J., Proffett J., Einaudi M., Zurcher L., Stavast W., Johnson D. & Barton M. 2005: Porphyry Deposits: Characteristics and Origin of Hypogene Features. *Economic Geology 100th Anniversary Volume*, 251–298. https://doi.org/10.5382/AV100.10

Seedorff E., Barton M.D., Stavast W.J.A. & Maher D.J. 2008: Root zones of porphyry systems: Extending the porphyry model to depth. *Economic Geology* 103, 939–956. https://doi.org/10.2113/gsecongeo.103.5.939

Siani M.G. & Lentz D.R. 2022: Lithogeochemistry of various hydrothermal alteration types associated with precious and base metal epithermal deposits in the Tarom-Hashtjin metallogenic province, NW Iran: Implication for regional exploration. *Journal of Geochemical Exploration* 232, 106903. https://doi.org/10.1016/j.gexplo.2021.106903

Sillitoe R.H. 2010: Porphyry copper systems. *Economic Geology* 105, 3–41. https://doi.org/10.2113/gsecongeo.105.1.3

Sinclair W.D. 2007: Porphyry Deposits: Mineral Deposits of Canada: A Synthesis of Major Deposit-Types, District Metallogeny, the Evolution of Geological Provinces, and Exploration Methods. *Geological Association of Canada, Mineral Deposits Division, Special Publication* 5, 223–243.

Stefanova E. 2009: Genetic peculiarities of quartz of the porphyry-copper deposit Elatsite. *PhD thesis*, *Sofia University*, Sofia, 1–157 (in Bulgarian).

Stefanova E., Driesner T., Zajacz Z., Heinrich C., Petrov P. & Vasilev Z. 2014: Melt and fluid inclusions in hydrothermal veins: The magmatic to hydrothermal evolution of the Elatsite porphyry Cu–Au deposit, Bulgaria. *Economic Geology* 109, 1359–1381. https://doi.org/10.2113/econgeo.109.5.1359

Stefanova E., Georgiev S., Peytcheva I., Marchev P., von Quadt A., Raicheva R., Gerdjikov I., Kouzmanov K., Boyce A. & Vennemann T. 2023: Sulfide trace element signatures and S- and Pb-isotope geochemistry of porphyry copper and epithermal gold-base metal mineralization in the Elatsite–Chelopech ore field (Bulgaria). *Minerals* 13, 630. https://doi.org/10.3390/min13050630

Strashimirov S., Petrunov R. & Kanazirski M. 2002: Porphyry-copper mineralisation in the Central Srednogorie zone Bulgaria. *Mineralium Deposita* 37, 587–598. https://doi.org/10.1007/s00126-002-0275-6

Strashimirov S., Bogdanov K. & Kehayov R. 2003: Porphyry systems of the Panagyurishte ore region. *Economic Geology* 36, 47–77. https://doi.org/10.5382/GB.36.03

Tarkian M., Hünken U., Tokmakchieva M. & Bogdanov K. 2003: Precious-metal distribution and fluid-inclusion petrography of the Elatsite porphyry copper deposit, Bulgaria. *Mineralium Deposita* 38, 261–281. https://doi.org/10.1007/s00126-002-0336-x

Taylor R.P. & Fryer B.J. 1980: Multiple-stage hydrothermal alteration in porphyry copper systems in northern Turkey: the temporal interplay of potassic, propylitic, and phyllic fluids. *Canadian Journal of Earth Sciences* 17, 901–926. https://doi.org/10.1139/e80-088

Trashliev S. 1961: On genesis and age of barite deposit Kashana, Pirdopsko. *Review of the Bulgarian Geological society* 22, 245–252 (in Bulgarian).

Ulrich T. & Heinrich C. 2002: Geology and alteration geochemistry of the porphyry Cu–Au deposit at Bajo de la Alumbrera, Argentina. *Economic Geology* 97, 1865–1888. https://doi.org/10.2113/gsecongeo.96.8.1719

van Dongen M., Weinberg R. F. & Tomkins A. G. 2010: REE-Y, Ti, and P remobilization in magmatic rocks by hydrothermal alteration during Cu–Au deposit formation. *Economic Geology* 105, 763–776. https://doi.org/10.2113/gsecongeo.105.4.763

von Quadt A., Peytcheva I., Kamenov B., Fanger L., Heinrich C. & Frank M. 2002: The Elatsite porphyry copper deposit in the Panagyurishte ore district, Srednogorie Zone, Bulgaria: U–Pb zircon geochronology and isotope-geochemical investigation of the magmatism and ore genesis. In: Blundell D.J., Neubauer F. & von Quadt A. (Eds): The Timing and Location of Major Ore Deposits in an Evolving Orogen. *Geological Society London, Special Publication* 204, 119–135.

von Quadt A., Moritz R., Peytcheva I. & Heinrich C. 2005: Geochronology and geodynamics of Late Cretaceous magmatism and Cu–Au mineralization in the Panagyurishte region of the Apuseni–Banat–Timok–Srednogorie belt, Bulgaria. *Ore Geology Reviews* 27, 95–126. https://doi.org/10.1016/j.oregeorev.2005.07.024

Wiewióra A. & Weiss Z. 1990: Crystallochemical classification of phyllosilicates based on the unified system of projection of chemical composition: II. The chlorite group. *Clay minerals* 25, 83–92.

Zhang F., Williamson B., Ullmann C. & Hughes H. 2023: Chemical changes during endoskarn and porphyry-style alteration and Cu Fe exoskarn mineralization in the Tonglushan system, eastern China. *Resource Geology* 73, e12319. https://doi.org/10.1111/rge.12319

Zimmerman A., Stein H., Markey R., Fanger L., Heinrich C., von Quadt A. & Peytcheva I. 2003: Re–Os ages for the Elatsite Cu–Au deposit, Srednogorie zone, Bulgaria. In: Eliopoulos et al. (Eds): Mineral exploration and sustainable development. *Millpress*, Rotherdam, 1253–1256.

Electronic supplementary material is available online:

https://geologicacarpathica.com/data/files/supplements/GC-77-1-Georgieva_Supplement.docx